

ModelingModelling the regional sensitivity of snowmelt, soil moisture and streamflow generation to climate over the Canadian Prairies using a basin classification approach

Zhihua He¹, Kevin Shook¹, Christopher Spence², John W. Pomeroy¹ and Colin Whitfield^{3,4}

¹Centre for Hydrology, University of Saskatchewan, Saskatoon, Saskatchewan, Canada

²Environment and Climate Change Canada, Saskatoon, Saskatchewan, Canada

³School of Environment and Sustainability, University of Saskatchewan, Saskatoon, Saskatchewan, Canada

⁴Global Institute for Water Security, University of Saskatchewan, Saskatoon, Saskatchewan, Canada

Abstract

This study evaluated the effects of climate perturbations on snowmelt, soil moisture and streamflow generation in small Canadian Prairie basins using a modelingmodelling approach based on classification of basin biophysical and hydraulic parameters characteristics. Seven basin classes that encompass the entirety of the Prairie ecozone in Canada were determined by cluster analysis of biophysicalthese characteristics. Individual semi-distributed virtual basin (VB) models representing these classes were parameterized in the Cold Regions Hydrological Model (CRHM) platform, which includes modules for snowmelt and sublimation, soil freezing and thawing, actual evapotranspiration (ET), soil moisture dynamics, groundwater recharge and depressional storage dynamics including fill and spill runoff generation and variable connected areas. Precipitation (P) and temperature (T) perturbation scenarios covering the range of climate model predictions for the 21st century were used to evaluate climate sensitivity of hydrological processes in individual land cover and basin types across the Prairie ecozone. Results indicated that snow accumulation in wetlands had a greater sensitivity to P and T than that in croplands and grasslands in all the-basin types. Wetland soil moisture was also more sensitive to T than the cropland and grassland soil moisture. Jointly influenced by land cover distribution and local climate, basin-average snow accumulation was more sensitive to T in the drier and grassland-characterized basins than in the wetter basins dominated by cropland, whilst basin-average soil moisture was most sensitive to T and P perturbations in basins typified by pothole depressions and broad river valleys. Annual streamflow had the greatest sensitivities to T and P in the dry and poorly connected Interior Grassland basins but the smallest in the wet and well-connected Southern Manitoba basins. The ability of P to compensate for warming-induced reductions in snow accumulation and streamflow was much higher in the wetter and cropland-dominated basins than in the drier and grassland-characterized basins, whilst decreases in cropland soil moisture induced by the maximum expected warming of 6 °C could be fully offset by P increase of 11% in all the-basins. These results can be used to 1) identify locations which had the largest hydrological sensitivities to changing

33 climate; and 2) diagnose underlying processes responsible for hydrological responses to expected climate
34 change. Variations of hydrological sensitivity in land cover and basin types suggest that different water
35 management and adaptation methods are needed to address enhanced water stress due to expected climate
36 change in different regions of the Prairie ecozone.

37 1. Introduction

38 The Canadian Prairies Ecozone occupies [approximately](#) 450,000 km² from Alberta in the west to
39 Manitoba in the east (Figure 1). This agricultural region features a semi-arid to sub-humid, cold, continental
40 climate with a long-term mean annual precipitation of less than 500 mm, approximately one-third of which
41 is snowfall (Shahabul Alam and Elshorbagy, 2015). The Prairies in their natural state were extensively
42 covered by grasslands and topographic depressions filled with wetlands. Now they are the most extensive
43 agricultural land base in Canada, whilst providing crucial habitat for waterfowl and other wetland and
44 grassland associated animals (Anteau et al., 2016; Zhang et al., 2021). Spring snowmelt is the major water
45 source of runoff in the Prairies and the extensive depressions play important roles in storing, evaporating
46 and transporting snow and surface runoff (Pomeroy et al., 2022; Fang and Pomeroy, 2009; Costa et al.,
47 2020; Unduche et al., 2018). Prairie hydrological states can vary widely from drought to deluge (Johnson
48 et al., 2005). Evaluating the sensitivity of Prairie hydrology to climate perturbation ~~would~~[can](#) help inform
49 adaptation of water management to future climate changes.

50 The Canadian Prairies are projected to experience relatively rapid climate change in the 21st century.
51 Air temperatures are projected to increase substantively during the next few decades. For example, mean
52 annual temperature is predicted to increase by 1.0 °C to 6.0 °C in most of the Prairies by 2100, compared
53 to 1986 – 2005 (Bush and Lemmen 2019). Similarly, results from regional climate models (RCMs) indicate
54 that mean annual temperatures in the Prairie Pothole region will increase by 1.8 °C to 4 °C by the end of
55 this century (Withey and van Kooten, 2011). However, projections of future precipitation are much less
56 certain. Johnson et al. (2005) reported that changes in Prairie precipitation in the 21st century could decrease
57 [by](#) 20% in some areas and increase [by](#) 20% in others, whilst Bush and Lemmen (2019) predicted that mean
58 annual precipitation will rise by up to 25% in the western Prairie but decrease by ~~—~~0.2% in the southern
59 Prairie (with differing seasonal responses), compared to 1986~~—~~2005. Jiang et al. (2017) projected that
60 seasonal precipitation in Alberta will change from ~~—~~25% to [±](#)36% by the end of 21st century, compared
61 to 1961~~—~~1990. Uncertainty in the projected precipitation is attributed to the mismatch between the coarse
62 resolutions of general circulation models (GCMs) or RCMs and the scale of convective precipitation
63 generation in the Prairies (Zhang et al., 2011), which is not always well parameterized in climate models
64 (Zhang et al., 2021). The large uncertainty in climate model projections can restrict their practical
65 application for predicting future hydrology in the Prairies. An alternative method is to add changes to
66 baseline temperature and precipitation conditions informed by ensembles of GCM and RCM projections to
67 represent the range of uncertainty in the projections. This delta method has proven useful to assess
68 hydrological sensitivity to climate perturbations in the Canadian Prairies and nearby regions (Rasouli et al.,
69 2019; ~~Spence et al., 2022a~~[Spence et al., 2022a](#)). Particularly, Kienzle et al. (2012) perturbed 30-year baseline precipitation

70 and temperature observations to represent future climate conditions and provide insights into the responses
71 of seasonal streamflow regimes in the Cline River basin, Alberta. MacDonald et al. (2012) used the delta
72 method to shift baseline climate to represent monthly perturbations in precipitation and temperature and
73 showed the sensitivity of snowpack to climate changes in the North Saskatchewan River basin. However,
74 these sensitivity analyses were limited to small basins or portions of the Prairies (e. g., Spence et al. 2022a).
75 Comparison of the hydrological sensitivity to climate change across the entire Canadian Prairie region has
76 not yet been rigorously conducted.

77 Hydrological models can be effective tools for quantifying the hydrological impacts of climate
78 change. However, complex hydrography such as in the Prairie Pothole Region make hydrological
79 ~~modeling~~modelling in Prairie basins a highly challenging task (Gray, 1970; Fang et al., 2010; Unduche et
80 al., 2018). First, snowmelt and rainfall runoff may not necessarily contribute flow to the basin outlet, as
81 wetlands store surface runoff until their storage capacity is exhausted. As extra runoff only spills and flows
82 to the basin outlet once no storage capacity remains, the uplands only connect to the channel when
83 downstream wetlands are filled (Shaw et al., 2012; Shook et al., 2015). The fill-spill runoff of wetlands and
84 the intermittent surface hydrological connection within Prairie basins specifically is poorly represented in
85 many hydrological models, as those models typically don't simulate physics of depressional storage
86 (Muhammad et al., 2019). Second, blowing snow and frozen soil infiltration strongly affect the generation
87 of snowmelt runoff in spring (Pomeroy et al., 1998). Snow is redistributed directly into prairie depressions
88 from surrounding agricultural fields (Pomeroy et al., 1993; Fang and Pomeroy, 2009). Infiltration of
89 snowmelt into frozen soil is complicated by multiple factors including snowpack accumulation, initial soil
90 moisture, and soil thermal properties (Gray et al., 2001). Physical representation of thermal dynamics of
91 frozen soil in a hydrological model is prerequisite for successful simulation of snowmelt runoff in the
92 Prairies (Pomeroy et al., 2007; Pomeroy et al., 2022). Third, the typical sparse observations of hydro-
93 meteorological data in the Prairies restrict opportunities to calibrate empirical hydrological models using
94 streamflow (St-Jacques et al., 2018). Streamflow records in the Prairie basins are typically intermittent and
95 characterized by long periods of zero flow (Whitfield et al., 2020), with many stream gauge stations
96 operated seasonally. The gauging network is extremely sparse and is considered to be insufficiently gauged
97 for regionalization of runoff (Samuel et al., 2013). ~~Since~~As streamflow in the region is dominated by spring
98 snowmelt runoff, any calibration from streamflow may bias parameters to certain hydrological processes
99 and seasons. Records of streamflow in the Prairies are therefore not necessarily useful for parameter
100 calibration. The complex hydrology of the Prairies highlights the need for physically-based hydrological
101 ~~modeling~~modelling approaches where parameters for calculation of snow redistribution, snowmelt runoff,
102 soil moisture, depressional storage and streamflow can be estimated based on basin hydrography and
103 biophysical properties.

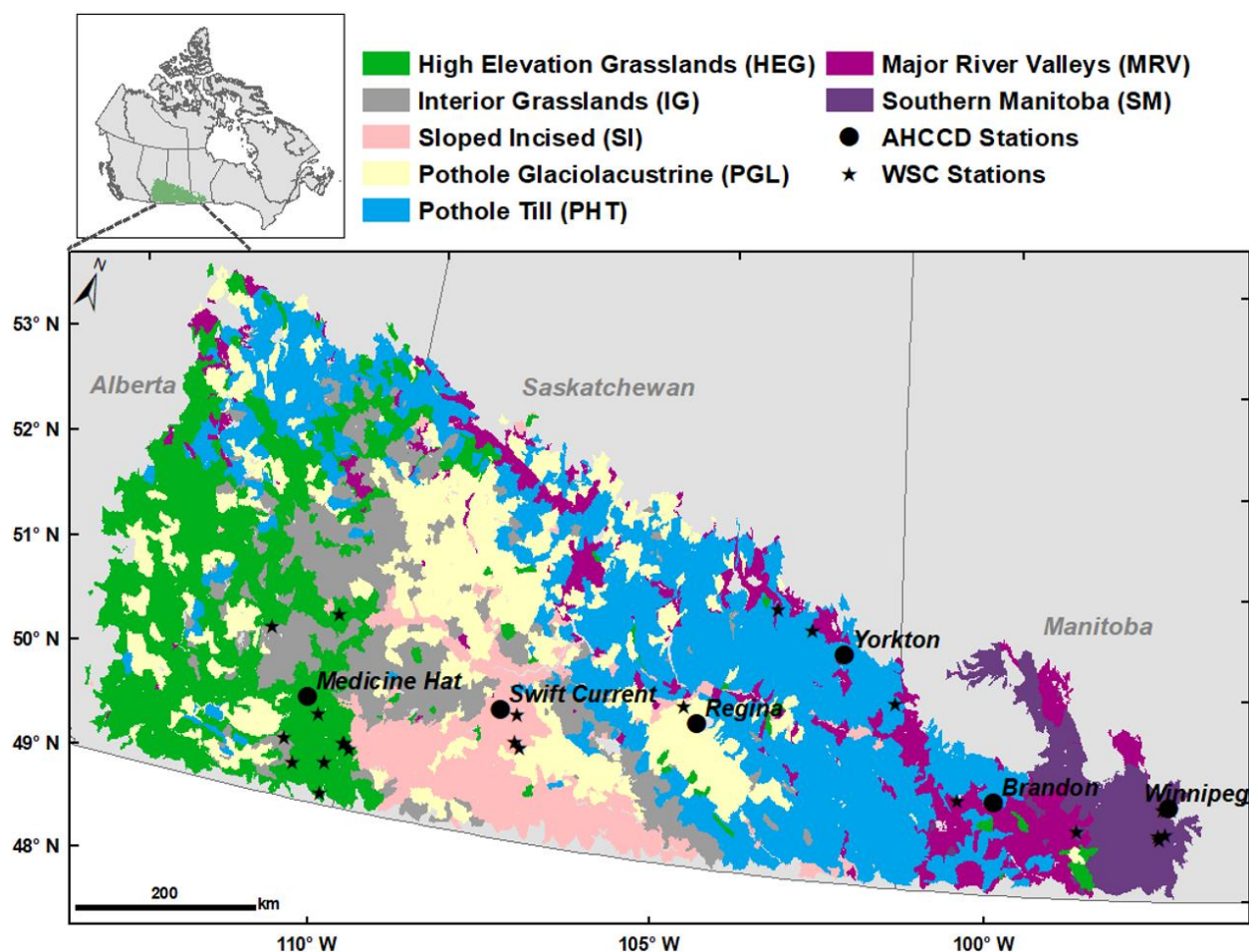
104 Building physically-based hydrological models over the entire Prairie ecozone is nonetheless
105 challenging due to dynamic contributing areas caused by geographically isolated wetlands (Pomeroy et al.,
106 2014; Unduche et al., 2018) resulting in poorly defined drainage basins (Pomeroy et al., 2010). A
107 virtualVirtual basin (VB) based modeling approachmodelling using hydrological response units (HRUs) to
108 represent the typical land cover and hydrographic land types in the Prairies wasprairies (Armstrong et al.,
109 2015), boreal forest (He and Pomeroy, 2023) and alpine basins (Lopez Moreno et al., 2020) has been
110 successfully used to examine the spatial variability of ET over the Prairies (Armstrong et al., 2015),
111 hydrological sensitivity to climate change and role of snow in governing hydrology, for example. Moreover,
112 VB modelingmodelling informed by basin classification (Wolfe et al., 2019) has been successfully applied
113 for assessing streamflow sensitivity to climate perturbation in the western part of the Prairies (Spence et al.,
114 2022a). ThisThe current study applies this hydrological modelingmodelling approach over the entire
115 Canadian Prairies with the aims of: (1) assessing and comparing hydrological sensitivity to climate by
116 evaluating how snow, soil moisture and runoff processes in different land cover types respond; (2)
117 quantifying and comparing the hydrological sensitivity to climate in all these seven different basin types across
118 the Prairies; and (3) assessing the degree to which precipitation increases can compensate for the
119 hydrological impacts of warming on Prairie hydrological processes.

120 2. Study area and basin classification

121 The Canadian Prairie region is in the south-central part of western Canada (N 49°–°–54°, W 90°–
122 W90°–115°, Figure 1), extending around 0.45 million km² across the Provinces of Alberta, Saskatchewan,
123 and Manitoba. Mean annual precipitation in the Prairies increases from west to east (Johnson and Poiani,
124 2016; Wolfe et al., 2019), from 300 mm to 610 mm (1970–2000). Mean annual air temperature over the
125 Prairies ranges from 1°C to 6 °C. The long and cold winter results in 30% of annual precipitation falling as
126 snow. Landscapes in the Prairies are, in general, flat, with millions of small wetland depressions embedded
127 within grassland and annual cropping lands (abbreviated as cropland landscapes hereafter). Wolfe et al.
128 (2019) classified approximately 41004200 headwater basins of, on average, ~100 km² across the Canadian
129 Prairies into seven biophysical basin classes.

130 Here, a slightly different classification from Wolfe et al. (2019) is used. This one does not include
131 climate variables in the basin classification but features the same seven classes (Figure 1), and is identical
132 to the one described by Spence et al. (2022a). Cropland is the main land use type in all the seven classes,
133 accounting for 40–65%. Pothole Till (PHT) is the largest class by area (120,881 km²), 65% of which is
134 covered by cropland. The other class dominated by cropland (64%) is Pothole Glaciolacustrine (PGL),
135 which spans 77,844 km². The classes of High Elevation Grasslands (HEG), Interior Grasslands (IG) and
136 Sloped Incised (SI) are characterized by high grassland fractions of 37–49%. HEG is the largest

137 grassland-characterized class (79,667 km²). The Major River Valleys (MRV) class (21,149 km²) is
 138 characterized by distinct valleys which cover 17% of the class area, and Southern Manitoba (SM) is the
 139 class with the fewest highly drained wetlands and the most extensive cropland (34,533 km²). Average
 140 depression coverage, associated with wetlands, ranges from 4% to 28% across the seven classes, with the
 141 largest coverage in PHT and PGL and the smallest coverage in IG. More details on the classification are
 142 provided by Wolfe et al. (2019).



143
 144 Figure 1. Map of the Prairie ecozone study area in south-central western Canada (inset) with basin classes
 145 and locations of AHCCD meteorological stations and Water Survey of Canada (WSC) streamflow
 146 stations. Note that areas in light grey are excluded from the analysis (due to large water bodies or urban
 147 coverage of the basin, or not being entirely within the study domain).

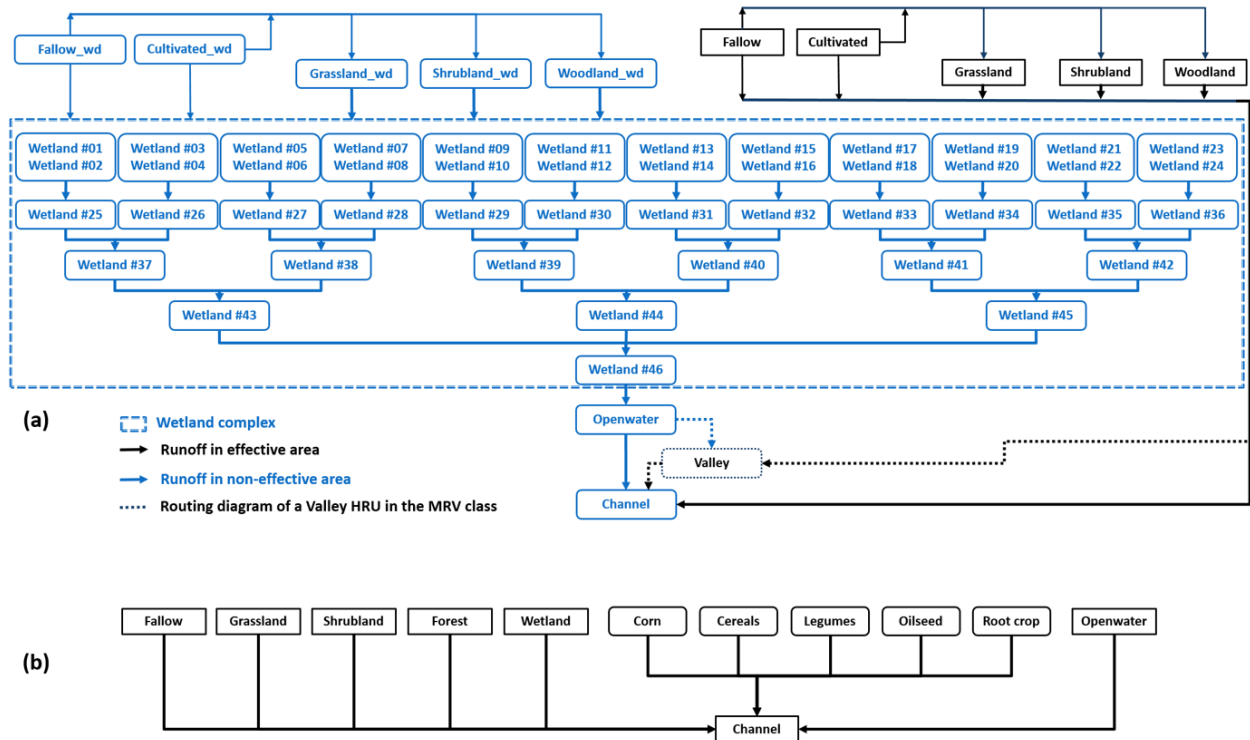
148 3. Methodology

149 3.1 Virtual basin (VB) based modeling approach modelling

150 To set up hydrological models in CRHM parsimoniously, the VBs were assigned an area of 100
 151 km², in accordance with the average area of the 4175 Prairie basins classified by Wolfe et al. (2019). Each
 152 VB consists of five upland covers of fallow fields, cultivated fields, grasslands, shrublands, woodlands, and

153 three downstream land types of depressions filled with wetlands, ~~open-water~~openwater bodies and stream
154 channels that were used to define HRUs (Spence et al. 2022a and b, Table 1, Figure 2). The HRU ~~area~~areal
155 fractions were derived from the results of the basin classification. [Summer fallowing is a declining
156 agricultural practice in the prairies, which is demonstrated by the small areal fraction of fallow in all the
157 basin types \(Table 1\)](#). In each VB except SM, the five upland covers were divided into two portions based
158 on the average effective drainage area of the class ~~(Table 1)~~. The effective part contributes runoff directly
159 to the channel, while the non-effective part routes runoff through a stylized wetland depression complex as
160 shown by HRUs with a suffix of ‘_wd’ in Figure 2a and Table 1. This was not done for SM owing to
161 widespread historical drainage of wetlands in this part of the prairie, with remaining wetlands typically
162 highly modified and lying adjacent to drainage ditches. The depression complex was characterized using
163 46 ‘wetland’ HRUs (Figure 2a, except SM), with every two upper wetlands contributing to one downstream
164 wetland (Pomeroy et al., 2014). Runoff from the depression complex was routed to the bottom openwater
165 HRU and then to the channel HRU. Areas of the 46 ‘wetland’ HRUs were estimated by generalized Pareto
166 distributions using parameters (i.e., β and ξ in Table 1) estimated in Wolfe et al. (2019) for the individual
167 basin classes (Shook et al., 2013).

168 For MRV, a unique valley HRU was inserted between the ~~open-water~~openwater HRU and channel
169 (see dashed lines in the bottom of Figure 2a). Runoff from the effective part was routed to the valley first,
170 and then to the channel HRU, whilst runoff from the depression complex flowed into the openwater HRU
171 first, and then to the valley and to the channel. This HRU represented the incised alluvial valley that is a
172 distinct feature of this basin class. In the SM basins, where warmer and wetter conditions allow a broader
173 diversity of agricultural crops that require specific parameterization, wetlands are typically connected to
174 the channel, much of which has been straightened via ditching. As such, the VB model representing these
175 basins was composed of twelve HRUs (one representing a wetland) with five distinctive crop HRUs (Figure
176 2b; Table 1), in which [vegetated](#) HRUs are connected to the channel HRU directly. Fractions of HRUs
177 representing different ~~land~~overland covers were determined as described above, with fractions of each
178 crop HRU derived from statistical analysis of land covers in two well-researched basins: South Tobacco
179 Creek (Mahmood et al., 2017) and the La Salle River (Cordeiro et al., 2017) in Manitoba’s Red River
180 Valley.



181
 182
 183
 184
 185

Figure 2. Routing orders of HRUs in the seven VB models created using CRHM. (a) VB models of HEG, IG, PHT, PGL, SI and MRV, where dashed arrow-lines indicate location of the valley HRU in MRV basins; and (b) VB model of SM. The ‘_wd’ notation is for the upland fraction that is in the wetland catena.

186 Table 1. HRU fractions for the VB models created by CRHM. The ‘_wd’ notation refers to the fraction
 187 that is in the wetland catena. -The long-term (1960–2006) mean air temperature and mean annual
 188 precipitation [are](#) observed at AHCCD stations ~~are for 1960–2006.~~ Basin-average effective area fraction,
 189 routing length and depressional storage capacity, parameters for deriving the wetland distribution, and
 190 crop types in the SM VB, as well as IDs of ~~selected~~[available](#) WSC stations for model evaluation are
 191 [listed](#)~~provided~~.

	HEG	IG	SI	PGL	PHT	MRV	SM
HRU fraction							
Fallow	0.004	0.002	0.01	0.002	0.002	0.003	4.9E–06
Fallow_wd	0.002	0.03	0.01	0.01	0.01	0.002	-
Cultivated	0.32	0.04	0.34	0.18	0.18	0.23	-
Cultivated_wd	0.13	0.38	0.15	0.46	0.47	0.17	-
Grassland	0.30	0.04	0.26	0.01	0.02	0.11	0.27
Grassland_wd	0.12	0.40	0.11	0.03	0.06	0.08	-
Shrubland	0.02	0.002	0.01	0.003	0.005	0.04	0.02
Shrubland_wd	0.01	0.02	0.01	0.01	0.01	0.03	-
Woodland	0.02	0.001	0.02	0.002	0.01	0.05	0.10
Woodland_wd	0.01	0.01	0.01	0.01	0.03	0.04	-
Wetlands	0.07	0.04	0.06	0.28	0.21	0.07	0.08
OpenWater	1.9E–06	3.4E–02	1.8E–06	3.3E–06	3.7E–06	1.7E–06	0.05
Valley	-	-	-	-	-	0.17	-
Channel	7.2E–03	7.2E–03	6.7E–03	3.0E–03	3.4E–03	9.9E–03	0.005
Effective area fraction	0.67	0.12	0.65	0.19	0.22	0.61	0.92
Mean routing length (m)	6757	7879	6677	6299	6537	5128	6256
Mean depression storage capacity (mm)	108	105	87	140	182	89	96
Representative AHCCD station	Medicine Hat	Swift Current	Swift Current	Regina	Yorkton	Brandon	Winnipeg
Mean annual T (°C)/ P (mm)	5.6/381	3.7/393	3.7/393	2.8/460	1.6/516	2.1/544	2.8/601
ID of selected WSC stations	05AF010; 11AB902; 05AH037; 11AB117; 11AB111; 11AB081; 11AA026; 05AH041	05CJ011; 05CK005	05JC004; 05JB007; 05JB005	05JF011	05ME007; 05MB012; 05MA022	05MG011; 05OF011	05OG009; 05MJ009; 05MJ007; 05OG010; 05OG003; 05MJ011
Wetland area generalized Pareto distribution parameters							
Scale (β)	2121.99	2813.42	2074.92	2195.37	2227.08	1910.83	-
Shape (ξ)	1.15	1.15	1.13	1.19	0.87	1.38	-

Crop HRU parameters in SM					
Crop type	Corn	Cereals	Legumes	Oilseed	Root Crop
HRU area fraction	0.01	0.26	0.03	0.18	0.003
Maximum LAI	5	3	3	4.5	3.75
Vegetation Height (m)	1	1.05	1.04	1	0.55

192 3.2 Cold Regions Hydrological Model (CRHM) and model parameterization

193 The CRHM platform is an object-oriented [modelingmodelling](#) system with modules representing
194 a wide range of hydrological processes (Pomeroy et al., 2007; 2022). Models created with CRHM have
195 proven successful for simulating streamflow in Canadian Prairie basins (Pomeroy et al., 2007, 2010, 2012,
196 2014; Fang et al., 2010; Mahmood et al., 2017; [CoreiroCordeiro](#) et al. 2017; 2022), and also in the US
197 northern great plains (Van Hoy et al., 2020). CRHM is strongly physically based and requires no parameter
198 calibration, and so is highly suitable for the VB [modelingmodelling](#) approach because the VB does not refer
199 to a specific gauged location that can be used for calibration (Pomeroy et al., 2013; Spence et al. 2022a). A
200 suite of modules was chosen to build and run the Prairie VB models in CRHM. The primary modules used
201 were (see more details on modules in Pomeroy et al., 2010): an observation input module to read the
202 meteorological forcing of air temperature, wind speed, relative humidity and precipitation data; a Prairie
203 Blowing Snow module to simulate the blowing snow redistribution and sublimation in the winter based on
204 vegetation height, topography and wind speed; an Energy-Budget Snowmelt module to estimate snowmelt
205 in spring according to the net balance between radiation and conductive and convective heat fluxes; a soil
206 module to represent soil moisture dynamics, infiltration of snowmelt and rain and Hortonian and Dunnian
207 runoff generation, thawing and freezing of soil water, and the filling and spilling of wetland depression
208 storage (Leibowitz and Vining, 2003); an ET module to simulate actual evaporation from unsaturated
209 surfaces using Granger and Gray’s (1990) combination method ET algorithm; Priestley and Taylor’s
210 energy-advection evaporation formula for saturated surfaces and [open-wateropenwater](#) bodies; and a
211 routing module using a Muskingum approach to route runoff [betweenfrom](#) HRUs to the basin outlet stream.

212 The strong physical basis of the CRHM modules allows the parameters to be estimated from field
213 studies described in the literature using the Deduction-Induction-Abduction approach (Pomeroy et al.,
214 2013). For each HRU in the VBs, parameters of vegetation height and leaf area index (LAI) were set to
215 represent the holding capacity of snow accumulation and canopy interception in winter. The vegetation
216 height for grassland and shrubland were set as 0.4 m and 1.5 m, respectively, adopting from Spence et al.
217 (2022a and b). Heights of crops range from 0.55 m to 1.05 m depending on the crop types (Table 1). The
218 maximum LAI for grassland and shrubland were set as 3 and 5 (Spence et al. 2022b), and crop LAI in the

219 SM VB ranged from 3 to 5. In addition, a depressional storage capacity was defined to govern the storage
220 and release of water in the wetland complex (Table 1). Storage capacities of wetlands were estimated based
221 on wetland HRU areas, using logarithmic or linear regression relations derived from LiDAR-measured
222 DEM data (Pomeroy et al., 2014). Soil properties in the HRUs were assumed to be loam as this was the
223 most common ~~as determined~~soil type for all basin classes in Wolfe et al. (2019). Routing distances across
224 each HRU to its downstream HRUs were estimated by a modified Hack's Law length-area relationship that
225 was derived from Smith Creek Research Basin in Saskatchewan by Fang et al. (2010) (Table 1).

226 3.3 Model application

227 Historical (~~1965–2005~~1960–2006) meteorological measurements from the Adjusted
228 Homogenized Climate Change Data (AHCCD, Mekis and Vincent, 2011) served as the baseline climate to
229 force the CRHM-based VB models (Figure 1). To reduce the impact of initial conditions, the first five years'
230 input was used to spin up the model running. This dataset is operated and continuously maintained by
231 Environment and Climate Change Canada's ~~department of~~ Meteorological Service of Canada.
232 Meteorological inputs include hourly observations of wind speed, relative humidity, surface air temperature,
233 and daily measurement of precipitation which was corrected for wind-undercatch of snowfall in gauges. To
234 reduce the computational effort, only one representative AHCCD station was chosen to force each
235 ~~class's~~class VB model, selected based on the proximity between the class centroid and the station location,
236 ~~as well as the availability of gauged meteorological data~~ (Table 1). Based on the long-term mean annual
237 precipitation at representative AHCCD stations and the ~~area~~areal fractions of grassland and cropland HRUs,
238 the seven basin types were divided into two groups: ~~one~~(1) is dry and grassland-characterized type including
239 HEG, IG and SI; ~~the other~~(2) is wet and cropland-dominated type for PGL, PHT, MRV and SM.

240 Daily streamflow measurements from Water Survey of Canada (WSC) stations that are close to the
241 representative AHCCD stations and gauge a basin which is >90% in the associated class (see stars in Figure
242 1 and IDs in Table 1) were selected for the VB model evaluation phase. As daily streamflows in the Prairies
243 are often zero, except during and following spring snowmelt, model performance was ~~based on~~evaluated
244 according to gauged annual and monthly streamflow for representative gauges. Snow depth measurements
245 on cropland taken in the South Tobacco Creek Research Basin by the WEBS Project of Agriculture and
246 Agri-~~Food~~Food Canada (e.g. Mahmood et al., 2017) were used to evaluate the model ability to simulate
247 snow accumulation in the SM class. Performance of the PHT VB model has proven acceptable in simulating
248 the inter-annual variability of depressional storage ~~by Spence et al. (2022b)~~(Spence et al. 2022b). Model
249 performance was primarily assessed by graphical assessment which includes comparing simulated and
250 observed data using various plots and visual representations for the agreement of broad range of values at
251 gauge sites, because traditional approaches for model assessment for basin-specific model applications to
252 instrumented basins are not appropriate here as the virtual basin does not directly align with any specific

real-world basin. For qualitative reference, we employed a simple metric of mass bias (MB) between the simulated and observed streamflow for performance evaluation (Eq. 1).

$$MB = \frac{\sum s}{\sum o} - 1 \quad (1)$$

where s and o are the simulated and observed annual streamflow, respectively.

3.4 Climate perturbation scenarios

To represent the potential future temperature (T) changes over the Prairies, seven T input scenarios were used to force the CRHM-based VB models to reflect predictions from an ensemble of climate models for the 21st century. This included a baseline scenario using historical T observations from the representative AHCCD stations, and six perturbation scenarios with warming from 1 °C to 6 °C with an increment of 1 °C. Five precipitation (P) input scenarios were used to represent potential future changes in P as reported by Bush and Lemmen (2019) and Johnson et al. (2005): a baseline scenario using historical P observations from the representative AHCCD stations, a drier scenario assuming that the P will decrease by up to 20% of the baseline observation, and three wetter scenarios with P increasing by 10%, 20% and 30%, respectively. To examine the synergistic impacts of combined P and T perturbations on VB outputs, the five P scenarios were combined with the seven T scenarios, resulting in 35 climate input scenarios.

3.4.3.5 Sensitivity analysis

The hydrological variables assessed include annual peak SWE (snow accumulation), annual snowmelt runoff, winter snow sublimation and spring snowmelt infiltration, growing season soil moisture (θ) in the shallow soil (recharge) layer and in the lower soil (deep root) layer, annual and monthly streamflow (Q) at the basin outlet, annual ET, annual maximum connected area fraction (CA) and mean daily depressional storage (SD). These variables were evaluated at the basin scale, while snow processes and soil moisture were further assessed for cropland, grassland and wetland HRUs (wetland results were area-weighted across the 46 individual HRUs). All variables except CA have the unit of mm. θ was assessed at a depth range of 0–12 cm for the recharge soil layer and 12–140 cm for the deep root soil layer, and 0–140 cm for the total soil layer. A Pearson Correlation Coefficient (CC_r) between Q sensitivity and the sensitivity of ET, SWE, θ and CA was used to investigate the major underlying contributor for Q sensitivity in the basin types of HEG, IG, SI, PGL, PHT and MRV. To facilitate comparisons between classes, hydrological sensitivity was quantified using the concept of elasticity (Eqs. 1–2). Elasticity (Schaake 1990) is used to assess the climatic sensitivity of hydrological processes, 2–3).

$$TES = [(M - m)/m] \times 100/\Delta T \quad (2)$$

$$PES = [(M - m)/m]/[(P_s - P_b)/P_b] \quad (3)$$

where, ΔT refers to the degree (°C) change in T , P_s is the P amount in the perturbed scenario, and P_b is the baseline P amount. M is the hydrological variable value forced by perturbed T or P scenarios, and m refers

286 to the corresponding variable value forced by baseline T and P inputs. In this study, as the hydrological
 287 models were forced by a range of P and T perturbations, mean precipitation elasticity (PES) was thus
 288 estimated as slope of the best fit line to scatter plots of $[(P_s - P_b)/P_b, (M - m)/m]$ derived from simulations in
 289 the 35 climate input scenarios. Similarly, mean temperature elasticity (TES) was estimated as the slope of
 290 the best fit line to scatter plots of $\{\Delta T, [(M - m)/m] \times 100\}$. The TES has units of $\% \text{ } ^\circ\text{C}^{-1}$, whilst PES is
 291 dimensionless.

292 Elasticity was first used to assess the climatic sensitivity of hydrological processes by Schaake
 293 (1990), referring to the percent change in a hydrological variable caused by a degree ($^\circ\text{C}$) warming or by
 294 1% change in P . Recently, Rasouli et al. (2022) used this metric to investigate hydrological sensitivity to
 295 climate perturbations in three North American mountainous basins, due to its advantage of standardizing
 296 the quantification of sensitivity at different locations. The temperature elasticity (TES) has a unit of $\% \text{ } ^\circ\text{C}^{-1}$,
 297 whilst precipitation elasticity (PES) is dimensionless.

$$298 \quad TES = [(M - m)/m] \times 100 / \Delta T \quad (1)$$

$$299 \quad PES = [(M - m)/m] / [(P_s - P_b)/P_b] \quad (2)$$

300 where, ΔT refers to the degree ($^\circ\text{C}$) change in T , P_s is the P amount in the perturbed scenario, and P_b is the
 301 baseline P amount. M is the hydrological variable value forced by perturbed T or P scenarios, and m refers
 302 to the corresponding variable value forced by baseline T and P inputs. In this study, as the hydrological
 303 models were forced by a range of P and T perturbations, mean PES was thus estimated as slope of the best
 304 fit line to scatter plots of $[(P_s - P_b)/P_b, (M - m)/m]$ derived from simulations in the 35 climate input scenarios.
 305 Similarly, mean TES was estimated as the slope of the best fit line to scatter plots of $\{\Delta T, [(M - m)/m] \times 100\}$.

306 7.4. Results

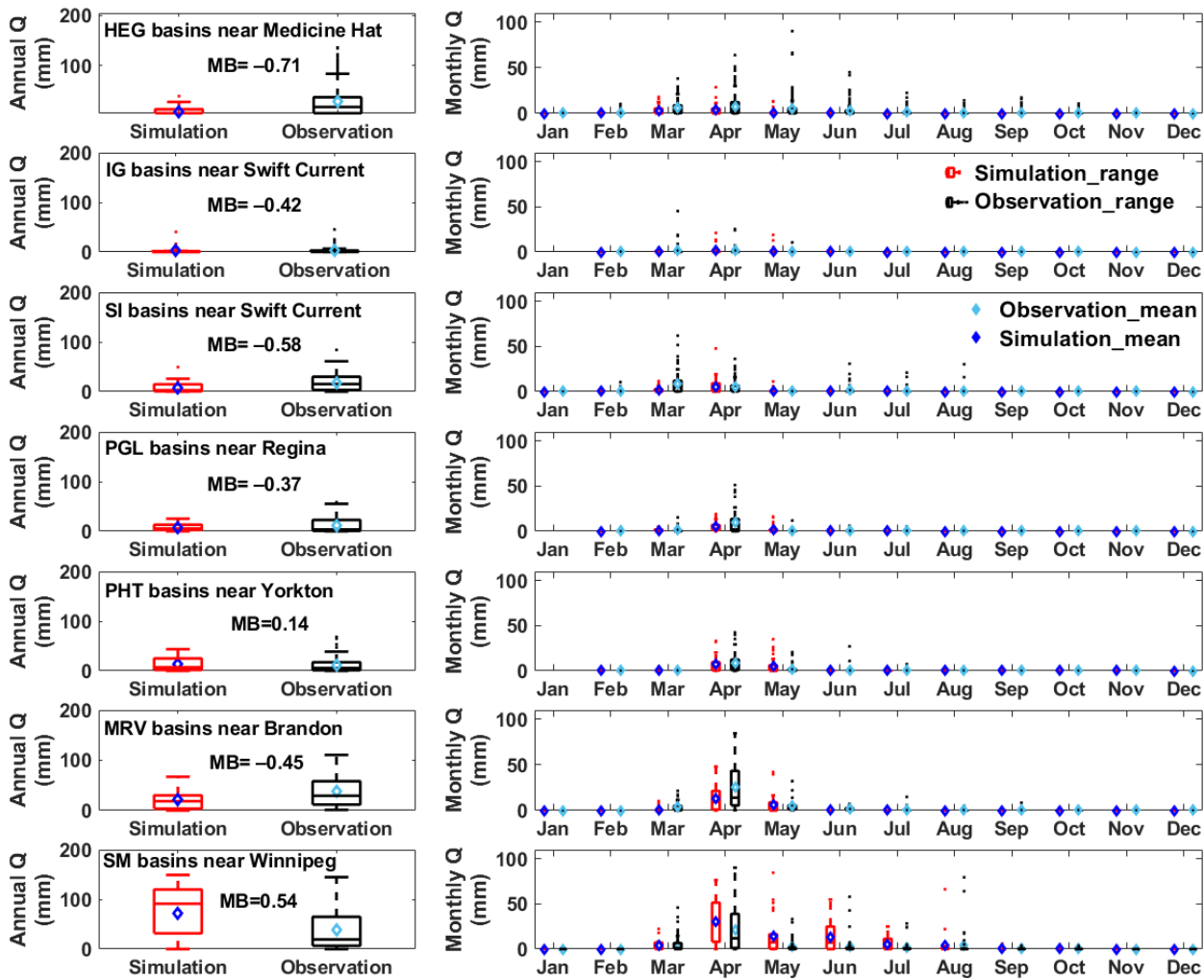
307 7.4.1 Model evaluation

308 Comparisons in Figure 3 indicate that streamflow simulations by the VB models aligned with
 309 observations of little or no streamflow in autumn and winter. The VB models also reasonably simulated
 310 that streamflow in the Prairies is dominated by runoff during snowmelt from March to May. The mean
 311 values and ranges of annual streamflow simulated by the VB models reflected observed annual streamflow
 312 amounts, (with the MB values ranging from -0.71 to 0.54), especially in the IG and PHT basins. In some
 313 cases at monthly scales (HEG (MB was only 0.14)). Simulated annual streamflow in March to September;
 314 other SM was larger than observations due to the overestimated monthly streamflow in April to June (MB
 315 was 0.54). In the remaining basins except SM in March to April, the VB models underestimated observed
 316 streamflow. Simulated monthly streamflow in SM was slightly larger than observations in April to June.

317 particularly in the primary melting months of March to April, indicated by the negative bias from -0.71 to
 318 -0.37 .

319 Bias In addition to model uncertainty, bias in simulated monthly and annual streamflow could be
 320 caused by associated with two factors. First, the AHCCD meteorological stations are generally located
 321 outside of the basins that were gauged by the selected WSC stations (Figure 1). Meteorological inputs
 322 measured at the AHCCD stations are therefore different from those that triggered runoff in the WSC gauged
 323 basins. This is most severe for summer rainfall, where misrepresentations of intense, but small spatial and
 324 temporal scale convective rainstorms occurring in the gauged basins, but missed in the AHCCD
 325 precipitation, likely contributed to underestimation of simulated streamflow in the warm seasons. Second,
 326 the CRHM-based VB hydrological models were structured and parameterized using the median
 327 characteristics of each class. The VB model parameters, such as the effective-area fraction, capacity of
 328 depressional storage, and land use types can differ from those in the specific WSC gauged basins,
 329 which likely led to some differences between simulated and observed streamflow.

330

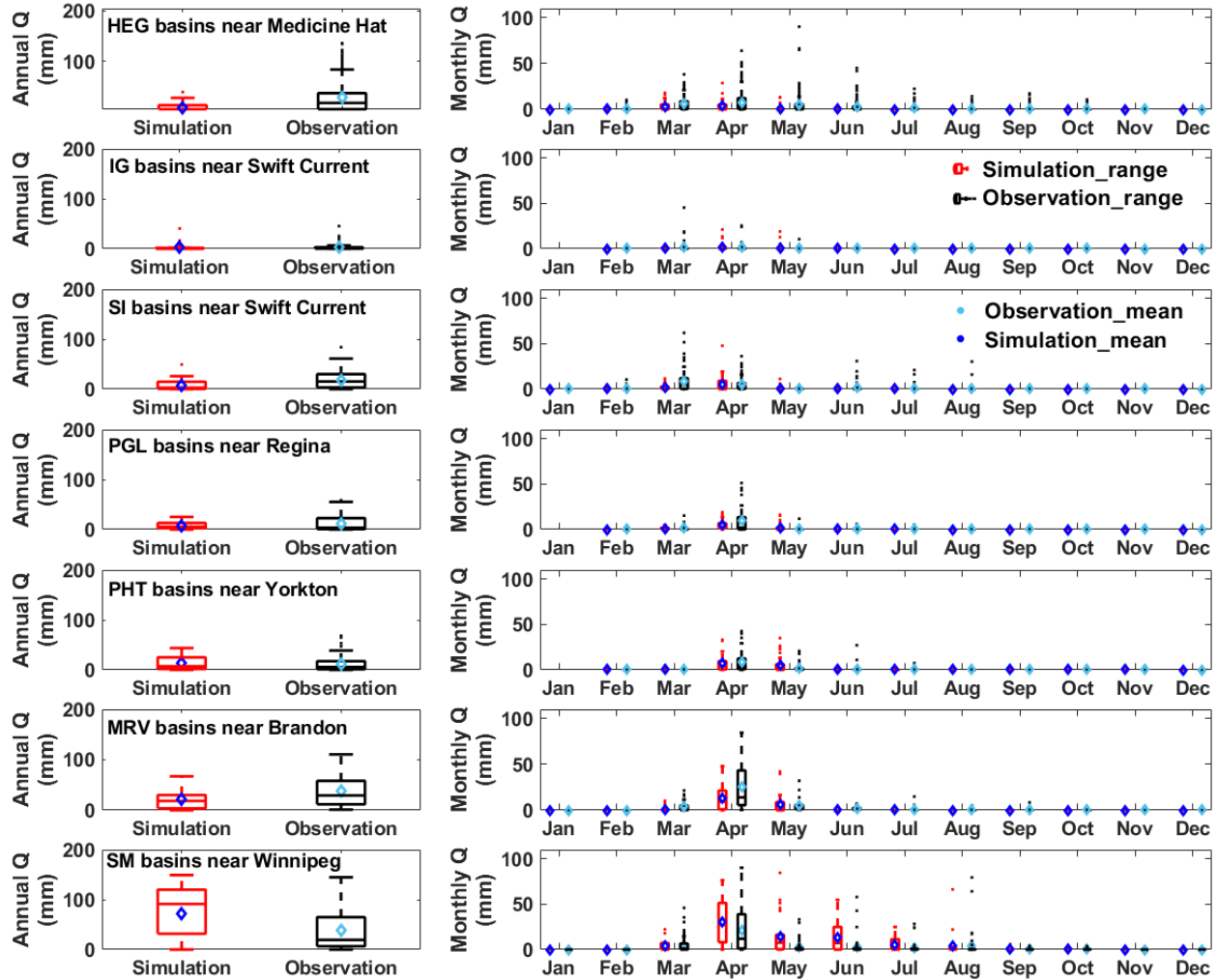


331 [Figure 3. Performance of the CRHM-based hydrological models in simulating annual \(left panel\) and](#)
332 [monthly \(right panel\) streamflow \(\$Q\$ \) over the Prairies \(1965–2006\). Boxplots refer to the inter-annual](#)
333 [variability in streamflow, and diamond dots represent the long-term mean values. \$MB\$ is mass bias](#)
334 [between simulated and observed annual streamflow.](#)

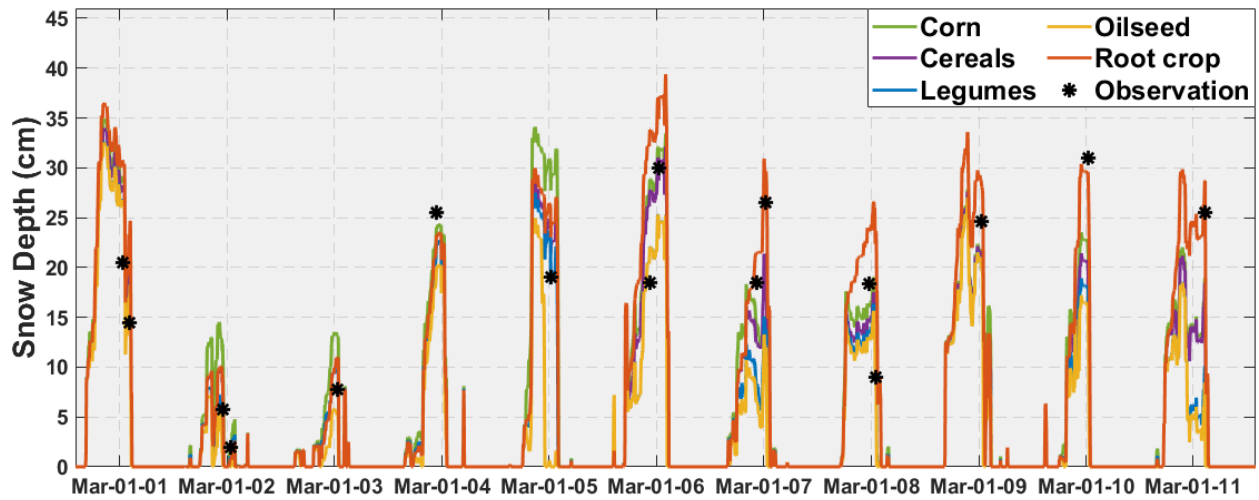
335 Simulated snow depth on multiple cropland sites replicated observations well in most years
336 between 2001 and 2011 in the SM class (Figure 4). Although the model slightly underestimated peak snow
337 depth in 2004 and 2010, observed snow depth in the remaining years ~~in general~~[generally](#) fell within the
338 simulation ranges at the various crop HRUs. The simulated snow accumulation showed reasonable pattern
339 that started in October and ended in March when melt and sublimation deplete the snowpack. Snow cover
340 disappeared from April and May due to strong melting. In addition to the evaluation in SM, the VB model
341 have proven effective in matching observed SWE at Red Deer, Alberta in the HEG class (Spence et al.,
342 2022a).

343 Model performance in simulating soil moisture was not evaluated by this work due to limited
344 availability of soil moisture measurement surrounding the representative AHCCD stations. ~~Instead,~~[The](#)
345 [CRHM-based VB models were](#)~~have been~~ verified as effective in simulating the soil moisture limited ET at
346 Lethbridge, Alberta and Central Saskatchewan (Armstrong et al. 2015). In the ET algorithm of CRHM,
347 actual ET rate was represented by a function of soil properties and moisture stress (Armstrong et al. 2010),
348 in which soil wetness was tracked for the ET calculation. Good agreement between cumulative curves of
349 observed and simulated ET in Armstrong et al. ~~(2010)~~ ~~and~~ ~~(~~ 2015) implied that the seasonality of soil
350 moisture could be reasonably represented in the CRHM VB models. Moreover, the CRHM soil module has
351 proven acceptable in reproducing observed volumetric soil moisture in Smith Creek [Research Basin](#),
352 Saskatchewan (Fang et al. 2010).

353 Considering that the CRHM-based VB models were not calibrated against observations and the
354 models were parameterized using typical values in the corresponding classes, and that they were forced
355 with climate data located at some distance from the monitored sites, [the](#) results in this and previous studies
356 ~~implied~~[imply](#) that the VB models are fit [for purpose](#) as tools to investigate hydrological sensitivity to
357 climate perturbations in the Prairies.



358
 359 **Figure 3.** Performance of the CRHM-based hydrological models in simulating annual (left panel) and
 360 monthly (right panel) streamflow (Q) over the Prairies (1965 – 2006). Boxplots refer to the inter-annual
 361 variability in streamflow, and diamond dots represent the long-term mean values.

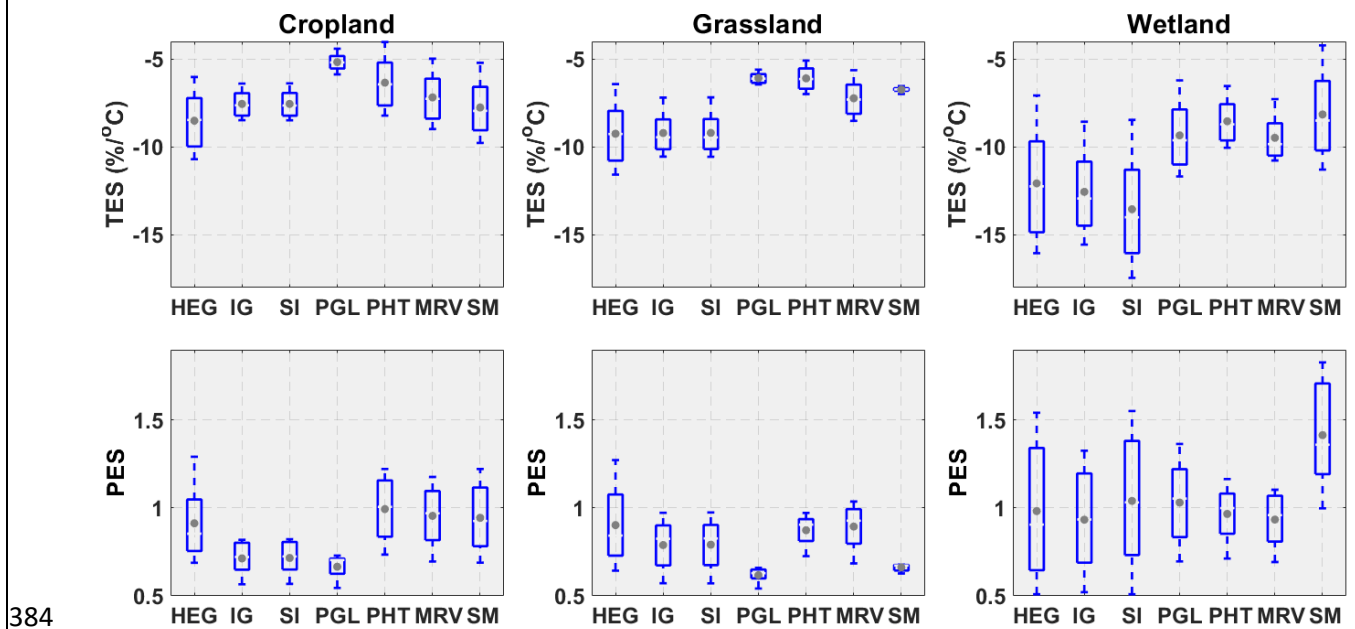


362
 363
 364
 365
 366
 367
 368
 369
 370
 371
 372
 373
 374
 375
 376
 377
 378
 379
 380
 381
 382
 383
 384
 385
 386
 387
 388
 389
 390
 391
 392
 393
 394
 395
 396
 397
 398
 399
 400
 401
 402
 403
 404
 405
 406
 407
 408
 409
 410
 411
 412
 413
 414
 415
 416
 417
 418
 419
 420
 421
 422
 423
 424
 425
 426
 427
 428
 429
 430
 431
 432
 433
 434
 435
 436
 437
 438
 439
 440
 441
 442
 443
 444
 445
 446
 447
 448
 449
 450
 451
 452
 453
 454
 455
 456
 457
 458
 459
 460
 461
 462
 463
 464
 465
 466
 467
 468
 469
 470
 471
 472
 473
 474
 475
 476
 477
 478
 479
 480
 481
 482
 483
 484
 485
 486
 487
 488
 489
 490
 491
 492
 493
 494
 495
 496
 497
 498
 499
 500
 501
 502
 503
 504
 505
 506
 507
 508
 509
 510
 511
 512
 513
 514
 515
 516
 517
 518
 519
 520
 521
 522
 523
 524
 525
 526
 527
 528
 529
 530
 531
 532
 533
 534
 535
 536
 537
 538
 539
 540
 541
 542
 543
 544
 545
 546
 547
 548
 549
 550
 551
 552
 553
 554
 555
 556
 557
 558
 559
 560
 561
 562
 563
 564
 565
 566
 567
 568
 569
 570
 571
 572
 573
 574
 575
 576
 577
 578
 579
 580
 581
 582
 583
 584
 585
 586
 587
 588
 589
 590
 591
 592
 593
 594
 595
 596
 597
 598
 599
 600
 601
 602
 603
 604
 605
 606
 607
 608
 609
 610
 611
 612
 613
 614
 615
 616
 617
 618
 619
 620
 621
 622
 623
 624
 625
 626
 627
 628
 629
 630
 631
 632
 633
 634
 635
 636
 637
 638
 639
 640
 641
 642
 643
 644
 645
 646
 647
 648
 649
 650
 651
 652
 653
 654
 655
 656
 657
 658
 659
 660
 661
 662
 663
 664
 665
 666
 667
 668
 669
 670
 671
 672
 673
 674
 675
 676
 677
 678
 679
 680
 681
 682
 683
 684
 685
 686
 687
 688
 689
 690
 691
 692
 693
 694
 695
 696
 697
 698
 699
 700
 701
 702
 703
 704
 705
 706
 707
 708
 709
 710
 711
 712
 713
 714
 715
 716
 717
 718
 719
 720
 721
 722
 723
 724
 725
 726
 727
 728
 729
 730
 731
 732
 733
 734
 735
 736
 737
 738
 739
 740
 741
 742
 743
 744
 745
 746
 747
 748
 749
 750
 751
 752
 753
 754
 755
 756
 757
 758
 759
 760
 761
 762
 763
 764
 765
 766
 767
 768
 769
 770
 771
 772
 773
 774
 775
 776
 777
 778
 779
 780
 781
 782
 783
 784
 785
 786
 787
 788
 789
 790
 791
 792
 793
 794
 795
 796
 797
 798
 799
 800
 801
 802
 803
 804
 805
 806
 807
 808
 809
 810
 811
 812
 813
 814
 815
 816
 817
 818
 819
 820
 821
 822
 823
 824
 825
 826
 827
 828
 829
 830
 831
 832
 833
 834
 835
 836
 837
 838
 839
 840
 841
 842
 843
 844
 845
 846
 847
 848
 849
 850
 851
 852
 853
 854
 855
 856
 857
 858
 859
 860
 861
 862
 863
 864
 865
 866
 867
 868
 869
 870
 871
 872
 873
 874
 875
 876
 877
 878
 879
 880
 881
 882
 883
 884
 885
 886
 887
 888
 889
 890
 891
 892
 893
 894
 895
 896
 897
 898
 899
 900
 901
 902
 903
 904
 905
 906
 907
 908
 909
 910
 911
 912
 913
 914
 915
 916
 917
 918
 919
 920
 921
 922
 923
 924
 925
 926
 927
 928
 929
 930
 931
 932
 933
 934
 935
 936
 937
 938
 939
 940
 941
 942
 943
 944
 945
 946
 947
 948
 949
 950
 951
 952
 953
 954
 955
 956
 957
 958
 959
 960
 961
 962
 963
 964
 965
 966
 967
 968
 969
 970
 971
 972
 973
 974
 975
 976
 977
 978
 979
 980
 981
 982
 983
 984
 985
 986
 987
 988
 989
 990
 991
 992
 993
 994
 995
 996
 997
 998
 999
 1000

363 Figure 4. Model performance in simulating snow depth observed at the South Tobacco Creek site in the
 364 SM class during 2001–2011.

365 **7.24.2 Snow sensitivity to climate perturbations**

366 Snow elasticity ~~was different among~~differed amongst land covers. For example, absolute *TES* of
 367 peak SWE in cropland and grassland were smaller than that in wetlands in all seven basin types, especially
 368 in the dry and grassland-characterized basins (Figure 5). In these classes, mean absolute *TES* of peak SWE
 369 in the wetland were around 13-% °C⁻¹, whilst they were only 8–9-% °C⁻¹ in the cropland and grassland (see
 370 ~~graygrey~~ dots in Figure 5). In the wet and cropland-dominated basins, mean absolute *TES* of peak wetland
 371 SWE were around 8-% °C⁻¹, whilst they were only 5–7-% °C⁻¹ in the cropland and grassland. The smaller
 372 absolute *TES* of peak SWE in the wet and cropland-dominated basins is because of their wetter baseline
 373 climate compared to the semi-arid grassland-characterized basins. The wetter climate resulted in a larger
 374 baseline SWE and thereby generated a smaller percentage decrease in SWE caused by warming. Absolute
 375 *TES* in cropland was smaller than grassland in the grassland-characterized basins and PGL, but larger in
 376 the remaining classes. Similarly, mean *PES* of peak SWE in wetland was larger than that in cropland and
 377 grassland (except PHT and MRV), especially in SM. The mean *PES* of peak SWE in wetlands was 1.4 in
 378 the SM class and close to 1.0 in the remaining classes, whilst both cropland and grassland mean *PES* were
 379 lower than 1.0 in all the basin types. Cropland *PES* in the grassland-characterized basins were smaller than
 380 grassland, but larger in the cropland-dominated basins. Variability in wetland snow elasticity forced by
 381 diverse *P* and *T* inputs was much larger than that in cropland and grassland (Figure 5), partly because snow
 382 accumulation in wetlands were strongly influenced by ~~snowwind~~ redistribution of snow to wetlands from
 383 all upland HRUs, ~~which~~. The blowing snow process was sensitive to climate ~~input~~inputs.



384

385 [Figure 5. Annual peak SWE temperature elasticity \(*TES*; top\) and precipitation elasticity \(*PES*; bottom\)](#)
386 [on varied land covers in the seven basin classes. Boxplots represent variability for the model runs forced](#)
387 [by diverse *P* and *T* perturbations.](#)

388 At the basin scale, peak SWE showed decreasing mean absolute *TES* from the drier and grassland-
389 characterized classes to the wetter and cropland-dominated classes, with the largest value of 9.2-% °C⁻¹ in
390 HEG and the smallest value of 7.1-% °C⁻¹ in PHT (Table 2). This could be [caused](#) partly ~~caused~~ by the
391 higher baseline peak SWE of the colder and wetter climates in the cropland-dominated classes (Table 1).
392 Despite that, wetlands showed larger absolute *TES* than other land covers in Figure 5, and wetland fractions
393 in the cropland-dominated classes were larger than those in the grassland-characterized basins (Table 1),
394 [results](#)). [Results](#) in Table 2 indicated that the *TES* of basin SWE was more determined by local climate
395 rather than land cover characteristics. The other winter snow process of sublimation, was more sensitive to
396 *T* than was SWE, showing the same decreasing tendency from grassland to cropland dominated basins. [The](#)
397 *TES* for snowmelt runoff and peak SWE were comparable among the grassland-characterized [basin](#) classes,
398 which can be expected as redistributed snow accumulation serves as the primary contributor to melt runoff.
399 However, in the cropland-dominated basins, the ~~*TES*~~ [absolute magnitude](#) of snowmelt runoff *TES* was lower
400 than that of peak SWE, which could be attributed to the large *TES* of snowmelt infiltration (Table 2). The
401 strong decrease in snowmelt infiltration in these classes could partly offset the decrease in snowmelt runoff
402 caused by warming. [Warming resulted in decreases in SWE, as indicated in Table 2. Consequently, both](#)
403 [infiltration and runoff resulting from snowmelt would be reduced by warming. Specifically, the decrease](#)
404 [in snowmelt infiltration was more pronounced in the cropland-dominated basin types compared to other](#)
405 [basin types \(Table 2\). This implies that a larger fraction of snowmelt runoff occurred in the warming](#)
406 [scenarios in these basins, which helped to lessen the reduction in snowmelt runoff.](#)

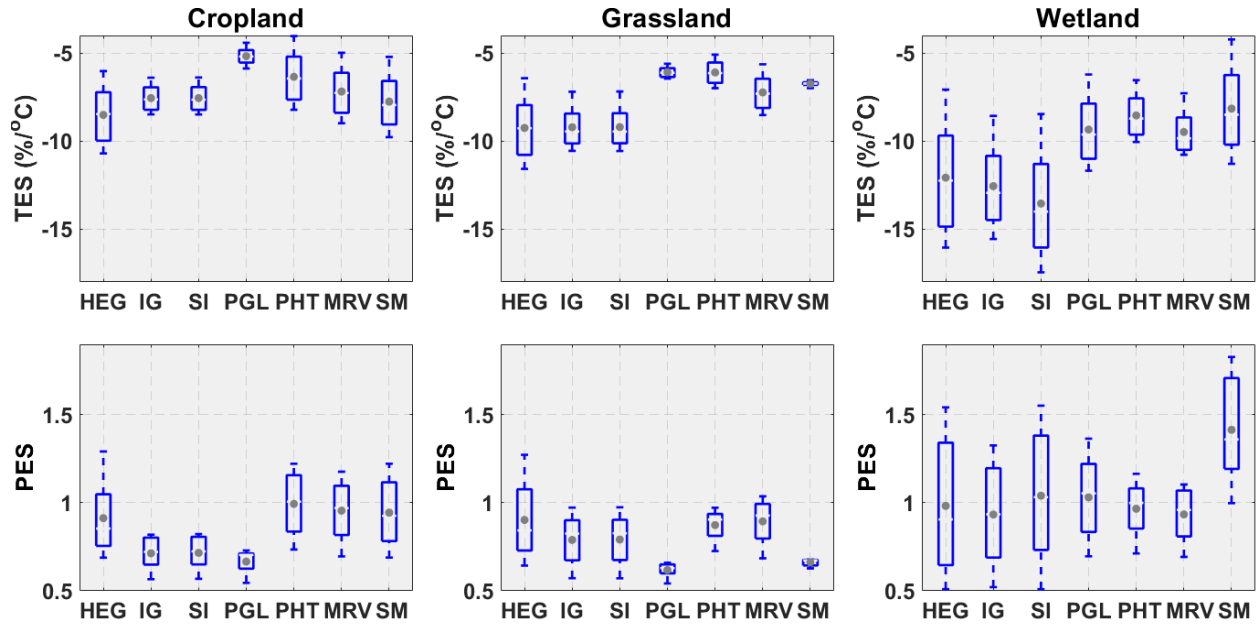


Figure 5. T and P elasticities of annual peak SWE on varied land covers in the seven basin classes.

Boxplots are for the inter-annual variability.

Table 2. Mean elasticities of basin-average snow processes/variables to warming and P rising forced by 35 climate input scenarios.

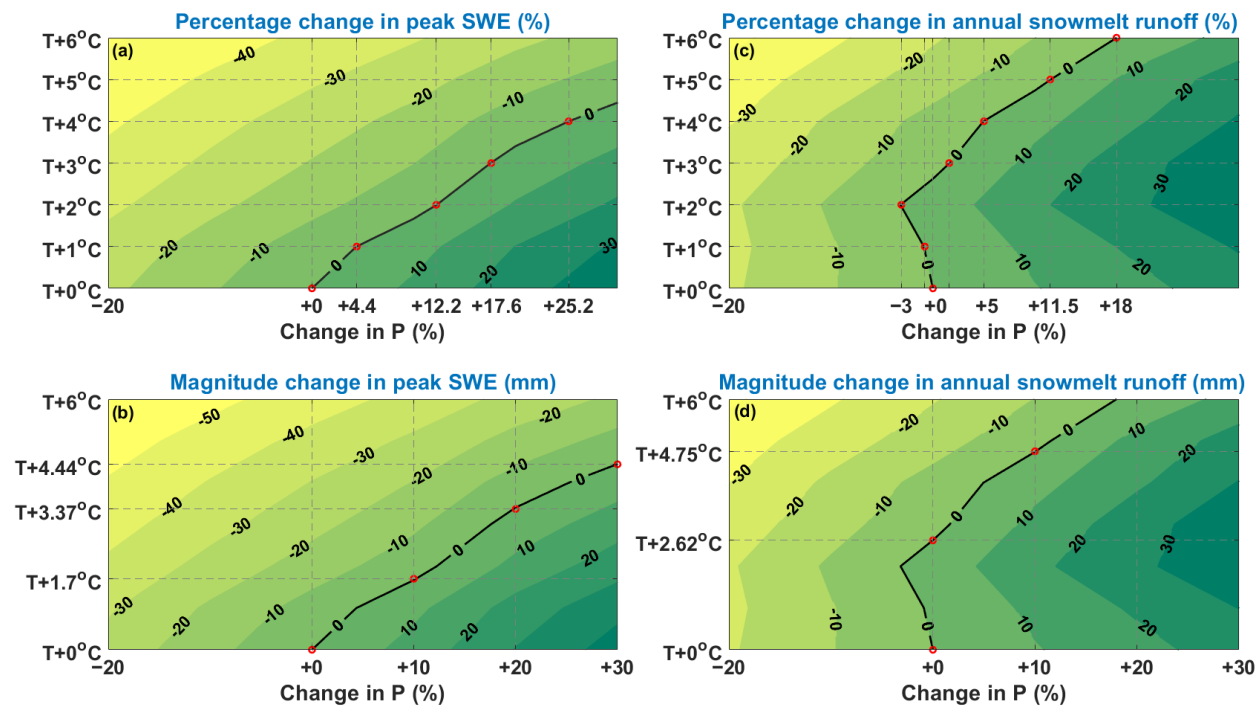
	<u>HEG</u>	<u>IG</u>	<u>SI</u>	<u>PGL</u>	<u>PHT</u>	<u>MRV</u>	<u>SM</u>
<u>T elasticity (TES, % $^{\circ}C^{-1}$)</u>							
<u>Peak SWE</u>	<u>-9.2</u>	<u>-8.9</u>	<u>-9.0</u>	<u>-7.3</u>	<u>-7.1</u>	<u>-7.6</u>	<u>-7.8</u>
<u>Snow sublimation</u>	<u>-18.1</u>	<u>-15.3</u>	<u>-16.2</u>	<u>-10.8</u>	<u>-10.6</u>	<u>-10.7</u>	<u>-9.1</u>
<u>Snowmelt runoff</u>	<u>-9.6</u>	<u>-9.7</u>	<u>-10.0</u>	<u>-5.4</u>	<u>-3.1</u>	<u>-4.9</u>	<u>-5.9</u>
<u>Snowmelt infiltration</u>	<u>-2.6</u>	<u>-1.8</u>	<u>-1.7</u>	<u>-4.6</u>	<u>-9.2</u>	<u>-5.7</u>	<u>-4.0</u>
<u>P elasticity (PES)</u>							
<u>Peak SWE</u>	<u>0.9</u>	<u>0.8</u>	<u>0.8</u>	<u>0.8</u>	<u>1.0</u>	<u>0.9</u>	<u>0.9</u>
<u>Snow sublimation</u>	<u>1.4</u>	<u>1.3</u>	<u>1.4</u>	<u>1.4</u>	<u>1.0</u>	<u>1.0</u>	<u>0.8</u>
<u>Snowmelt runoff</u>	<u>1.2</u>	<u>1.1</u>	<u>1.2</u>	<u>1.1</u>	<u>1.2</u>	<u>1.3</u>	<u>1.1</u>
<u>Snowmelt infiltration</u>	<u>0.3</u>	<u>0.3</u>	<u>0.3</u>	<u>0.1</u>	<u>0.2</u>	<u>0.1</u>	<u>0.1</u>

PES of snow sublimation was larger than 1.0 in the dry and grassland-characterized classes and PGL (Table 2), which indicated that snow sublimation was limited by snowfall availability in these classes. When P increased and generated more snowfall, sublimation showed a larger percentage increase rate than P . This could explain why PES of peak SWE was lower than 1.0, because of the enhanced snow loss via sublimation. In contrast, snowmelt infiltration was controlled by the rate of soil thawing associated with T in the melting season rather than the availability of snow meltwater in the Prairie basins. Although increased P resulted in larger snowmelt, PES of snowmelt infiltration was smaller than 1.0 because of the restriction

419 by frozen soil. As a result, *PES* of snowmelt runoff was larger than 1.0 because of the increased snowmelt
 420 availability for surface runoff generation (Table 2). Compared to *TES*, *PES* of snow processes showed
 421 smaller variations across the seven classes.

422 Table 2. Mean elasticities of basin average snow processes/variables to warming and *P* rising forced by
 423 35 climate input scenarios. *TES* and *PES* are for temperature elasticity and precipitation elasticity,
 424 respectively.

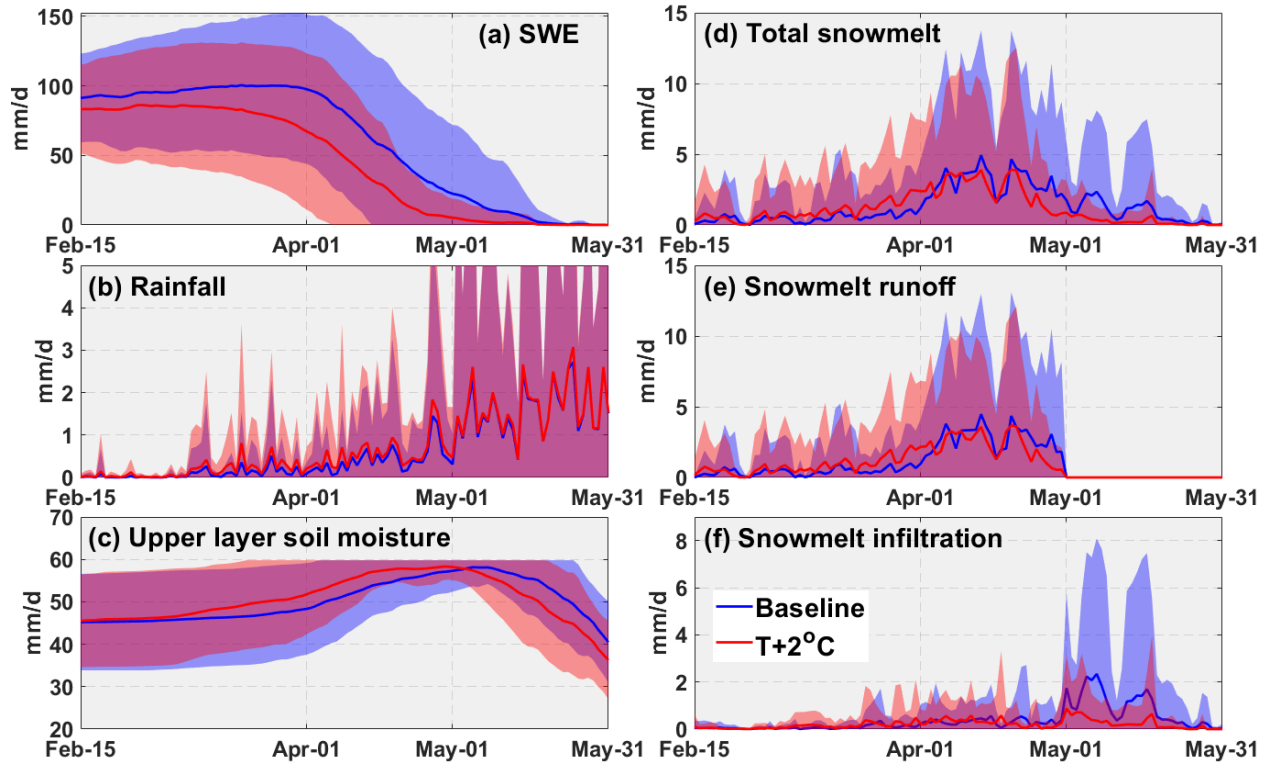
<i>TES</i> (% °C ⁻¹)	HEG	IG	SI	PGL	PHT	MRV	SM
Peak SWE	-9.2	-8.9	-9.0	-7.3	-7.1	-7.6	-7.8
Snow sublimation	-18.1	-15.3	-16.2	-10.8	-10.6	-10.7	-9.1
Snowmelt runoff	-9.6	-9.7	-10.0	-5.4	-3.1	-4.9	-5.9
Snowmelt infiltration	-2.6	-1.8	-1.7	-4.6	-9.2	-5.7	-4.0
<i>PES</i>							
Peak SWE	0.9	0.8	0.8	0.8	1.0	0.9	0.9
Snow sublimation	1.4	1.3	1.4	1.4	1.0	1.0	0.8
Snowmelt runoff	1.2	1.1	1.2	1.1	1.2	1.3	1.1
Snowmelt infiltration	0.3	0.3	0.3	0.1	0.2	0.1	0.1



425
 426 Figure 6. Combined effects of *T* and *P* perturbations on annual peak SWE and snowmelt runoff in
 427 the PHT class. Red dots on the upper panel show where the effects of warming scenarios were offset by
 428 percentage changes in *P*, and those on the lower panel show where the effects of *P* rising scenarios were
 429 offset by warming degrees in *T*.

430 Effects of expected warming on peak SWE (i.e., percentage and magnitude changes in SWE
431 caused by warming) can be partially offset by increased P within its possible future range in the Canadian
432 Prairies: (Figure 6). Using the results from the PHT class as an example (because this basin class has the
433 largest areal extent among the seven classes), decreases in peak SWE caused by warming from 1-°C to 4 °C
434 can be completely offset by the gains from P increases ranging from 4.4% to 25.2% (Figure 6a). The
435 maximum expected increase of 30% in future P , however, cannot fully offset the decrease in SWE caused
436 by warming higher than 5 °C. On the other hand, increases in SWE associated with P increases of 10%,
437 20% and 30% can be offset by warming of 1.7 °C, 3.37 °C and 4.44 °C, respectively (Figure 6b). With
438 warming of 6 °C, the decreases in snowmelt runoff can be fully offset if P increases by 18% (Figure 6c).
439 On the other hand, offsetting the increase in snowmelt runoff created with a P increase of 10% requires
440 warming of 4.75 °C (Figure 6d). P increases greater than 20% cannot be fully offset by warming lower than
441 6 °C.

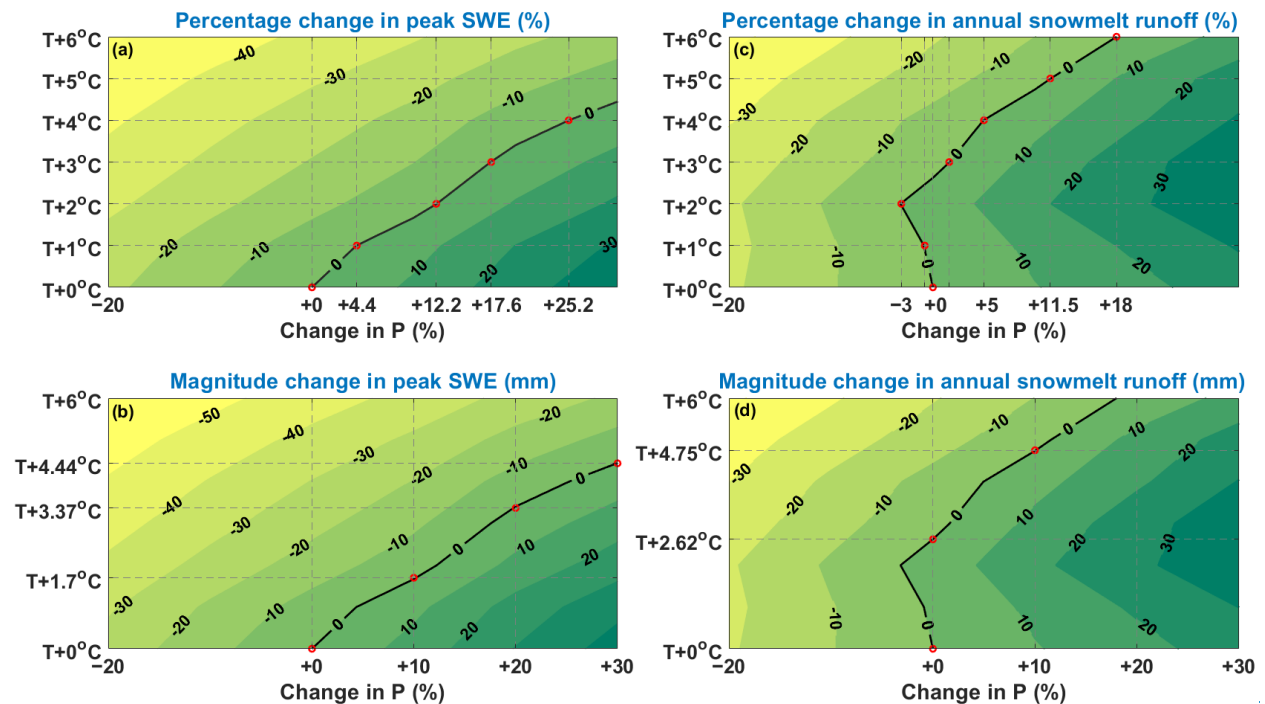
442 It is noted that snowmelt runoff increases slightly with warming of 1–2 °C in the PHT class (Figures
443 6c-d). This phenomenon could be caused by restricted-increased surface runoff fraction of snowmelt with
444 warming (Figure 7). With a warming of 2°C, a reduction in annual peak SWE and snowfall by 14.3 mm
445 (14%) and 20 mm (12%), respectively, was predicted (Figure 7a). Total rainfall increased by 20 mm (5.5%)
446 (Figure 7b). However, snowmelt surface runoff increased by 3.9 mm (3.9%), accompanied by a decrease
447 of 20 mm (40%) in snowmelt infiltration with warming, when ice lenses can form from spring melts
448 preceding full snowmelt (Figure 7), and more rain on snow events in warming(refer to Figures 7e-f).
449 Snowmelt infiltration was strongly constrained by antecedent conditions before May 1st (Figure 7c). In the
450 warmer scenarios (Fang and Pomeroy, 2007; Mahmood et al. 2017). With 2 °C warming, snowmelt runoff
451 in March was larger than, snowmelt initiated and concluded earlier, with a majority of the snowpack
452 melting away before May 1st at which date the soil layer started to thaw and soil moisture started to decrease
453 (Figures 7a, and 7c-d). The thawed soil layer after May 1st greatly facilitated snowmelt infiltration in the
454 baseline runoff due to raised T (Figure 7a). In April, warming scenario, during which considerable snowmelt
455 was still occurring after May 1st. The longer melting period extending to the thawing season in the baseline
456 scenario resulted in more ice lenses due to early melting and rain (Figure 7b). Snowmelt infiltration was
457 thus strongly restricted in the warming scenario (Figure 7c). Therefore, effects of warming of 1 – 2 °C on
458 snowmelt-a larger fraction of snowmelt infiltration, whereas the shorter melting period mainly falling within
459 the frozen soil season generated a larger fraction of surface runoff would be enhanced by P rising but be
460 offset by P decreases up to 3% (for snowmelt).



461

462

Figure 6e.



463

464

465

466

Figure 6. Combined effects of T and P perturbations on annual peak SWE and 7. Comparisons of daily snow accumulation and melt, snowmelt runoff in the PHT class. Red dots on the upper panel show where the effects of warming and infiltration, rainfall, and soil moisture in two T input scenarios were

offset by percentage changes in P , and those on the lower panel show where the effects of P rising scenarios were offset by warming degrees in T .

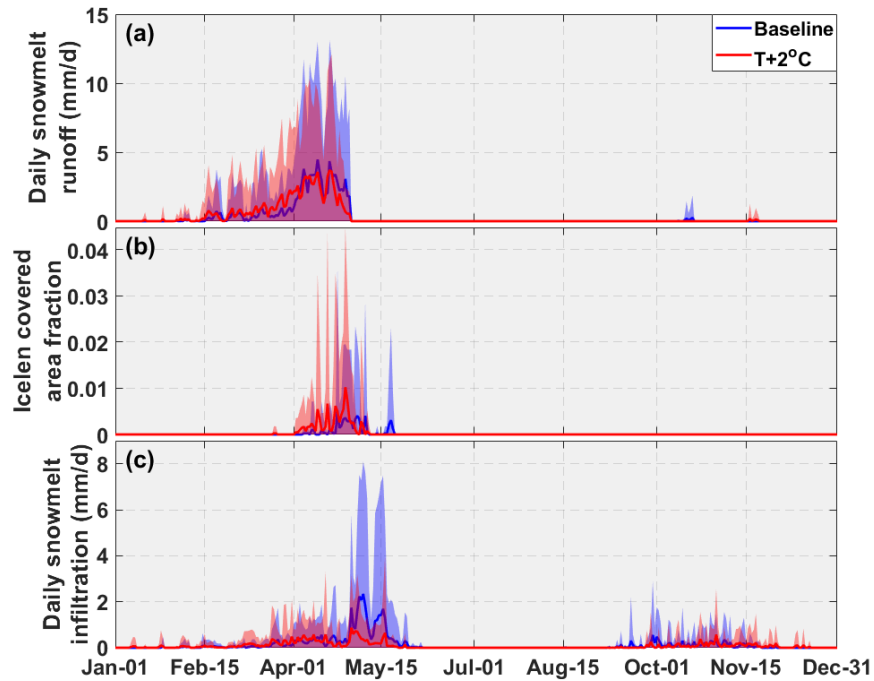


Figure 7. Comparisons of daily snowmelt runoff, ice lens covered area fraction, and daily snowmelt infiltration in two T scenarios in the PHT class. Bands refer to the inter-annual variability, and solid lines are for represent the mean daily values during throughout the modelling period, whilst the modeling period bands indicate the range of values within the standard deviation (+/-).

The effectiveness of P to compensate for warming effects on peak SWE increased from the drier and grassland-characterized classes to the wetter and cropland-dominated classes (Table 3). To offset the effects of warming by 1 °C, 9.5–10.2% increases in P were required in the HEG, IG, and SI classes, whilst smaller increases of around 4.4% were required in the PHT, MRV, and SM classes. Meanwhile, a 30% increase in P would be able to offset the effects of warming up to 3 °C in the PGL, MRV, and SM classes and even 4 °C in the PHT class, whilst such an increase in P could only offset the effects of warming of up to 2 °C in the HEG, IG, and SI classes. In contrast, warming of around 1 °C can offset the effects of a 10% increase in P in the HEG, IG, and SI classes, whilst warming of higher than 1.5 °C is required in the PGL, PHT, MRV, and SM classes.

The 35 combined climate inputs resulted in varied decreases and increases in peak SWE across the basin types (Table 3). The maximum percentage increases in peak SWE due to increased P of 30% were around 30–41% over the entire region, whilst the maximum absolute increases ranged from 17 mm in IG to 44 mm in PHT. The maximum percentage decreases in peak SWE ranged from 51% to 62%, associated

487 with warming of 6 °C and 20% decrease in *P*; absolute decreases in this scenario ranged from 35 mm in IG
 488 to 65 mm in MRV.

489 **Table 3.** Required *P* increases (%) to offset the effects of warming ~~for~~and required warming degrees (°C)
 490 to offset *P* ~~rising~~changes on annual peak SWE, and the maximum increase and decrease
 491 (percentage/magnitude) in peak SWE caused by the 35 combined *P* and *T* perturbation scenarios.

	<u>HEG</u>	<u>IG</u>	<u>SI</u>	<u>PGL</u>	<u>PHT</u>	<u>MRV</u>	<u>SM</u>
Warming scenario	Required <i>P</i> <u>increases (%)</u> to offset warming (%)						
T +1°C	+10.2	+9.5	+9.8	+6.4	+4.4	+4.6	+4.3
T +2°C	+22.9	+22.8	+23.2	+13.5	+12.2	+12.7	+15.5
T +3°C	>+30	>+30	>+30	+23.0	+17.6	+20.5	+24.5
T +4°C	>+30	>+30	>+30	>+30	+25.2	>+30	>+30
T +5°C	>+30	>+30	>+30	>+30	>+30	>+30	>+30
T +6°C	>+30	>+30	>+30	>+30	>+30	>+30	>+30
<i>P</i> changes scenario	Required <i>T</i> <u>warming degrees (°C)</u> to offset <i>P</i> <u>rising (°C)changes</u>						
P -20%	NA	NA	NA	NA	NA	NA	NA
P +10%	+0.96	+1.05	+1.01	+1.5	+1.7	+1.64	+1.52
P +20%	+1.8	+1.8	+1.76	+2.78	+3.37	+2.92	+2.55
P +30%	+2.62	+2.56	+2.56	+3.62	+4.44	+3.93	+3.62
Maximum increase in SWE (%/mm)	40.9/26.2	29.6/17.0	30.3/17.6	32.7/29.5	37.5/44.4	35.3/42.6	34.1/35.0
Maximum decrease in SWE(%/mm)	-62.4/-39.9	-61.2/-35.2	-61.4/-35.7	-50.9/-45.8	-51.4/-60.8	-53.9/-65.1	-56.6/-58.3

492 The 35 combined climate inputs resulted in varied decreases and increases in peak SWE across the
 493 basin types (Table 3). The maximum percentage increases in peak SWE due to increased *P* of 30% were
 494 around 30–41% over the entire region, whilst the maximum magnitude increases ranged from 17 mm in IG
 495 to 44 mm in PHT. The maximum percentage decreases in peak SWE ranged from 51% to 62%, associated
 496 with warming of 6 °C and 20% decrease in *P*; magnitude decreases in this scenario ranged from 35 mm in
 497 IG to 65 mm in MRV.

498 **7.34.3 Soil moisture sensitivity to climate perturbations**

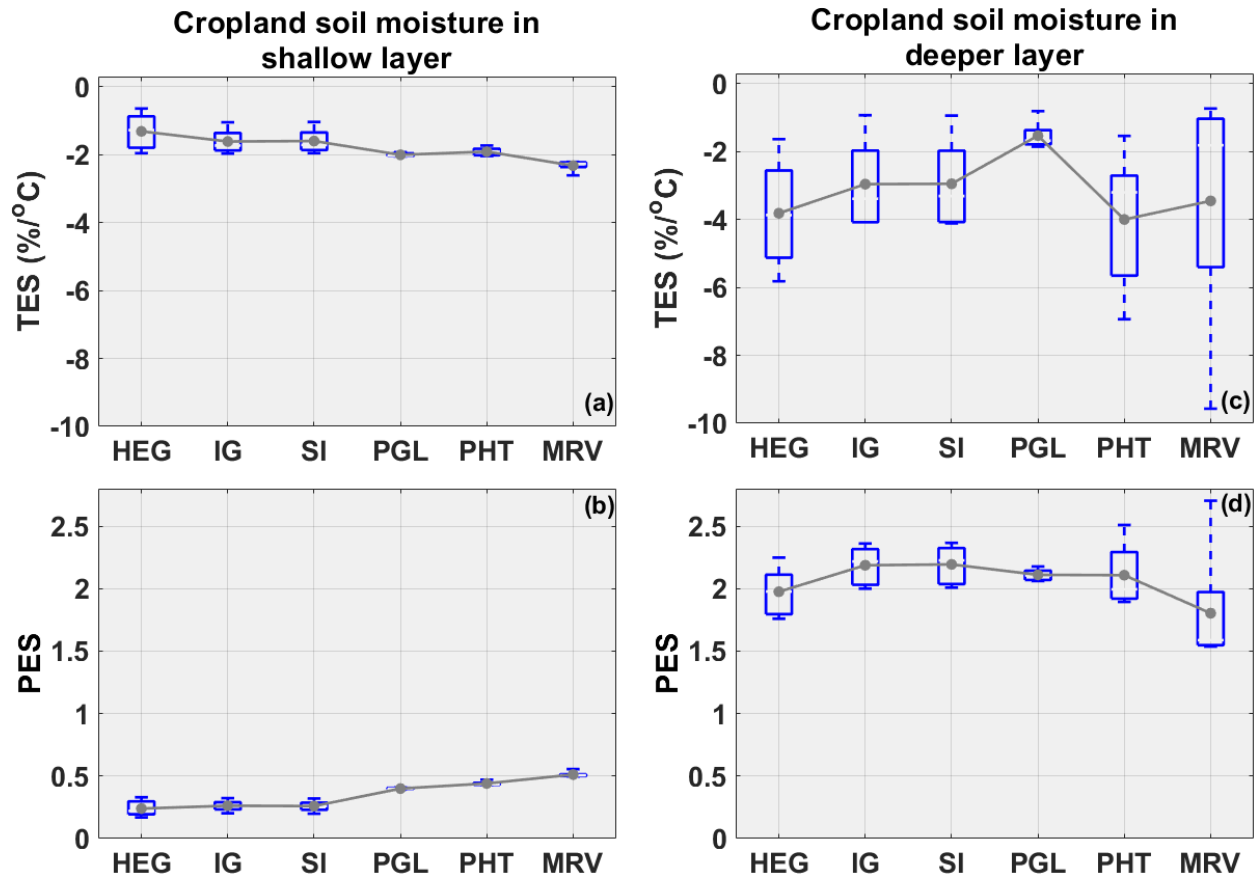
499 Growing season (May to September) soil moisture *TES* differed among land cover types in the
 500 basin classes (Table 4). The SM basins were excluded from this analysis, because the VB ~~model~~model's
 501 performance in simulating soil moisture in the eastern wet area has not been evaluated. Cropland soil
 502 moisture showed smaller mean absolute *TES* than in grassland and wetland along all the six evaluated
 503 classes. The maximum absolute *TES* for cropland soil moisture happened in PHT as 3.2 % °C⁻¹ followed
 504 by 2.5 % °C⁻¹ in MRV. The *TES* of grassland soil moisture was slightly higher, with a maximum absolute

505 value of 4.6 % °C⁻¹ in PHT. Wetland soil moisture showed the largest absolute *TES* among the land covers
 506 with the maximum of 9.3 % °C⁻¹ in SI and the minimum of 7.8 % °C⁻¹ in PHT. This could be explained by
 507 the fact that when their depressional storage dropped to zero, wetlands transitioned to bare surface, and soil
 508 moisture under those conditions was thus highly sensitive to warming. Variations in *TES* of the basin-
 509 average soil moisture among the basin types can be explained by the different land cover fractions in the
 510 classes (Table 1). For instance, HEG, IG and SI have high coverage of grassland; *TES* of basin-average soil
 511 moisture (around 3.2 % °C⁻¹) in these classes was thereby close to that of grassland soil moisture (around
 512 3.0 % °C⁻¹). In contrast, PGL and PHT had large land cover fractions of cropland and wetland, and their
 513 basin-average soil moisture *TES* (around 4.3 % °C⁻¹) was intermediary to values for cropland (1–3.2 % °C⁻¹)
 514 and wetland (7.9 % °C⁻¹).

515 **Table 4. Mean elasticities of growing season soil moisture (θ) to warming and *P* rising derived from**
 516 **simulations in 35 climate forcing scenarios.**

<i>TES</i> (% °C ⁻¹)	HEG	IG	SI	PGL	PHT	MRV
θ in cropland	-2.4	-1.9	-1.9	-1.0	-3.2	-2.5
θ in grassland	-3.1	-2.8	-3.0	-2.6	-4.6	-2.6
θ in wetland	-9.2	-8.9	-9.3	-7.9	-7.8	-8.3
Basin average θ	-3.4	-3.0	-3.0	-3.8	-4.8	-4.3
<i>PES</i>						
θ in cropland	1.5	1.8	1.8	1.8	1.9	1.6
θ in grassland	1.3	1.6	1.6	1.5	1.8	1.1
θ in wetland	1.8	1.3	1.6	1.6	1.7	1.4
Basin average θ	1.4	1.5	1.6	1.6	1.8	1.6

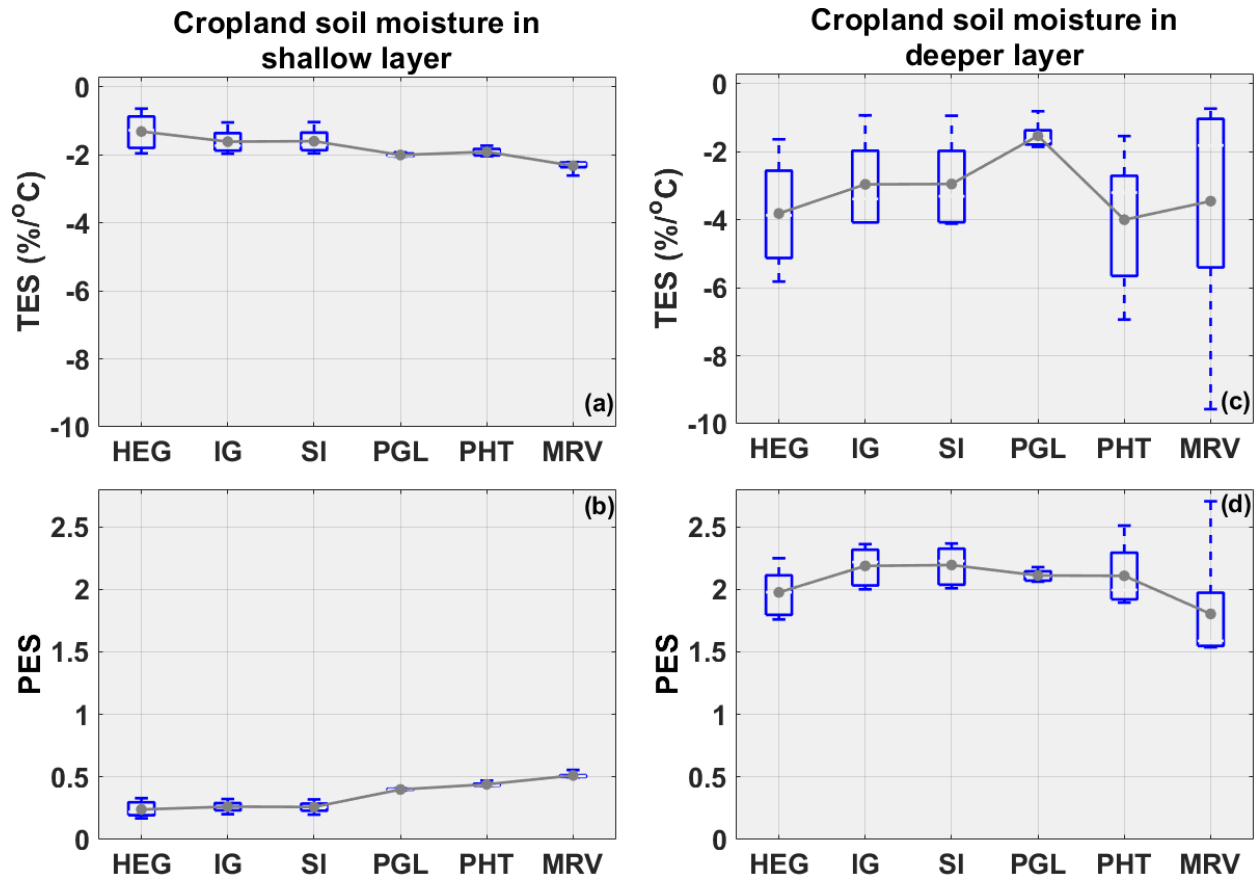
517 *PES* of growing season soil moisture, however, only exhibited slight differences across land covers
 518 and were typically larger than 1.0 which can be attributed to rainfall infiltration in the growing season being
 519 limited by the availability of rain input. In all the six classes, *PES* of cropland soil moisture ranged only
 520 from 1.5 to 1.9, and were between 1.1–1.8 and 1.3–1.8 in grasslands and wetlands, respectively (Table
 521 4). Again, basin-average soil moisture *PES* was close to that of grassland soil moisture in HEG, IG and SI,
 522 and was intermediary to values for cropland and wetland in the PGL, PHT and MRV classes.



523
524
525

Table 4. Mean elasticities of growing season's total soil moisture (θ) to warming and P rising derived from simulations in 35 climate forcing scenarios.

	<u>HEG</u>	<u>IG</u>	<u>SI</u>	<u>PGL</u>	<u>PHT</u>	<u>MRV</u>
<u>T elasticity ($TES, \% \text{ } ^\circ\text{C}^{-1}$)</u>						
<u>Cropland θ</u>	<u>-2.4</u>	<u>-1.9</u>	<u>-1.9</u>	<u>-1.0</u>	<u>-3.2</u>	<u>-2.5</u>
<u>Grassland θ</u>	<u>-3.1</u>	<u>-2.8</u>	<u>-3.0</u>	<u>-2.6</u>	<u>-4.6</u>	<u>-2.6</u>
<u>Wetland θ</u>	<u>-9.2</u>	<u>-8.9</u>	<u>-9.3</u>	<u>-7.9</u>	<u>-7.8</u>	<u>-8.3</u>
<u>Basin-average θ</u>	<u>-3.4</u>	<u>-3.0</u>	<u>-3.0</u>	<u>-3.8</u>	<u>-4.8</u>	<u>-4.3</u>
<u>P elasticity (PES)</u>						
<u>Cropland θ</u>	<u>1.5</u>	<u>1.8</u>	<u>1.8</u>	<u>1.8</u>	<u>1.9</u>	<u>1.6</u>
<u>Grassland θ</u>	<u>1.3</u>	<u>1.6</u>	<u>1.6</u>	<u>1.5</u>	<u>1.8</u>	<u>1.1</u>
<u>Wetland θ</u>	<u>1.8</u>	<u>1.3</u>	<u>1.6</u>	<u>1.6</u>	<u>1.7</u>	<u>1.4</u>
<u>Basin-average θ</u>	<u>1.4</u>	<u>1.5</u>	<u>1.6</u>	<u>1.6</u>	<u>1.8</u>	<u>1.6</u>



526

527

Figure 8. Comparisons of the climate elasticities of mean growing season soil moisture in cropland.

528

Boxplots refer to the variability forced by different P or T inputs, and dot-lines stand for the mean

529

elasticities.

530

531

532

533

534

535

536

537

538

539

Moisture in shallow ([recharge](#)) soil layers is of great interest to agricultural producers in the Canadian Prairies and is the source of crop growth by supplying water for dryland farming ET and plant productivity. As expected, moisture in shallow soils (Figures 8a,b) showed smaller mean absolute TES and PES than in deeper ([deep root](#)) soils (Figures 8c,d), because the shallow layer soil moisture capacity is much smaller and receives infiltrating waters first. Despite that, ~~the~~ [mean \$TES\$ \(absolute\) and \$PES\$ for shallow layer soil moisture](#) generally increased from the drier and grassland-characterized classes to the wetter and cropland-dominated classes, likely because that soil moisture in the shallow layer was easily depleted by ET in the dry sites. Deeper layer soil moisture response showed wide variability among the basin types. It had the largest absolute mean TES of around $4\% \text{ } ^\circ\text{C}^{-1}$ in the PHT class, whilst presenting the largest mean PES of 2.2 in the SI class.

540

Table 5. Required P increases (%) to offset the effects of warming ~~for~~ [and](#) required warming degrees ($^\circ\text{C}$)

541

to offset [changes in \$P\$ rising](#) on cropland's growing season [total](#) soil moisture, (θ) , and the maximum

542 increase and decrease (percentage/magnitude) in growing season's total soil moisture caused by the 35
 543 combined *P/T* perturbation scenarios.

	<u>HEG</u>	<u>IG</u>	<u>SI</u>	<u>PGL</u>	<u>PHT</u>	<u>MRV</u>
Warming scenario	Required <i>P</i> <u>increases (%)</u> to offset warming <u>(%)</u>					
T +1°C	+1.3	+2.1	+2.0	+1.6	+3.3	+2.8
T +2°C	+3.2	+3.1	+2.8	+2.8	+7.1	+5.7
T +3°C	+5.0	+4.1	+4.0	+3.9	+7.7	+5.8
T +4°C	+7.2	+5.5	+5.3	+4.6	+9.5	+7.2
T +5°C	+9.6	+7.2	+6.8	+5.0	+9.7	+7.9
T +6°C	+10.5	+7.7	+7.7	+5.4	+10.4	+7.8
<i>P</i> change scenario	Required <u>Δwarming degrees (°C)</u> to offset <i>P</i> <u>rising (°C) changes</u>					
P-20%	NA	NA	NA	NA	NA	NA
P +10%	+5.5	>+6	>+6	>+6	+5.5	>+6
P +20%	>+6	>+6	>+6	>+6	>+6	>+6
P +30%	>+6	>+6	>+6	>+6	>+6	>+6
Maximum increase in						
<u>soil moisture</u> θ	69.9/94.8	69.1/113.1	69.5/112.7	61.4/125.1	72.7/207.6	110.4/242.4
(%/mm)						
Maximum decrease						
in <u>soil moisture</u> θ	-34.1/-46.3	-37.2/-60.9	-37.1/-60.1	-40.6/-82.7	-51.6/-147.3	-24.1/-52.8
(%/mm)						

544 The effectiveness of *P* in compensating for the effects of warming on cropland's growing season
 545 soil moisture showed that a *P* increase of 10.5% was required to offset the effects of 6-°C warming in the
 546 HEG and PHT classes, (Table 5), which is much higher than the required increase of 5.4% in the PGL class
 547 (Table 5). The *P* increase in the IG and SI classes showed similar effectiveness, offsetting effects of 1-°C
 548 and 6-°C warming with increases of 2.0% and 7.7%, respectively. The MRV basins showed reduced
 549 effectiveness compared to IG and SI, indicated by the required *P* increases of 2.8%, and 7.8% to offset the
 550 effects of warming by 1 °C and 6 °C, respectively. In contrast, warming is not effective in compensating
 551 for the increases in soil moisture caused by more *P*. The maximum warming of 6 °C could only offset the
 552 effects of *P* increases up to 11% in any basin types. The maximum percentage ~~34%~~ increases in soil moisture
 553 by 30% *P* increase approached 61% in PGL, to as large as 110% in MRV. Maximum magnitude increases
 554 ranged from 95 mm to 242 mm in all basin types. The maximum decrease in soil moisture forced by 6 °C
 555 warming and 20% *P* decrease showed the percentage and magnitude values of 24–52% and 46–147 mm,
 556 respectively.

557 **7.44.4 Streamflow sensitivity to *P* and *T* climate perturbations**

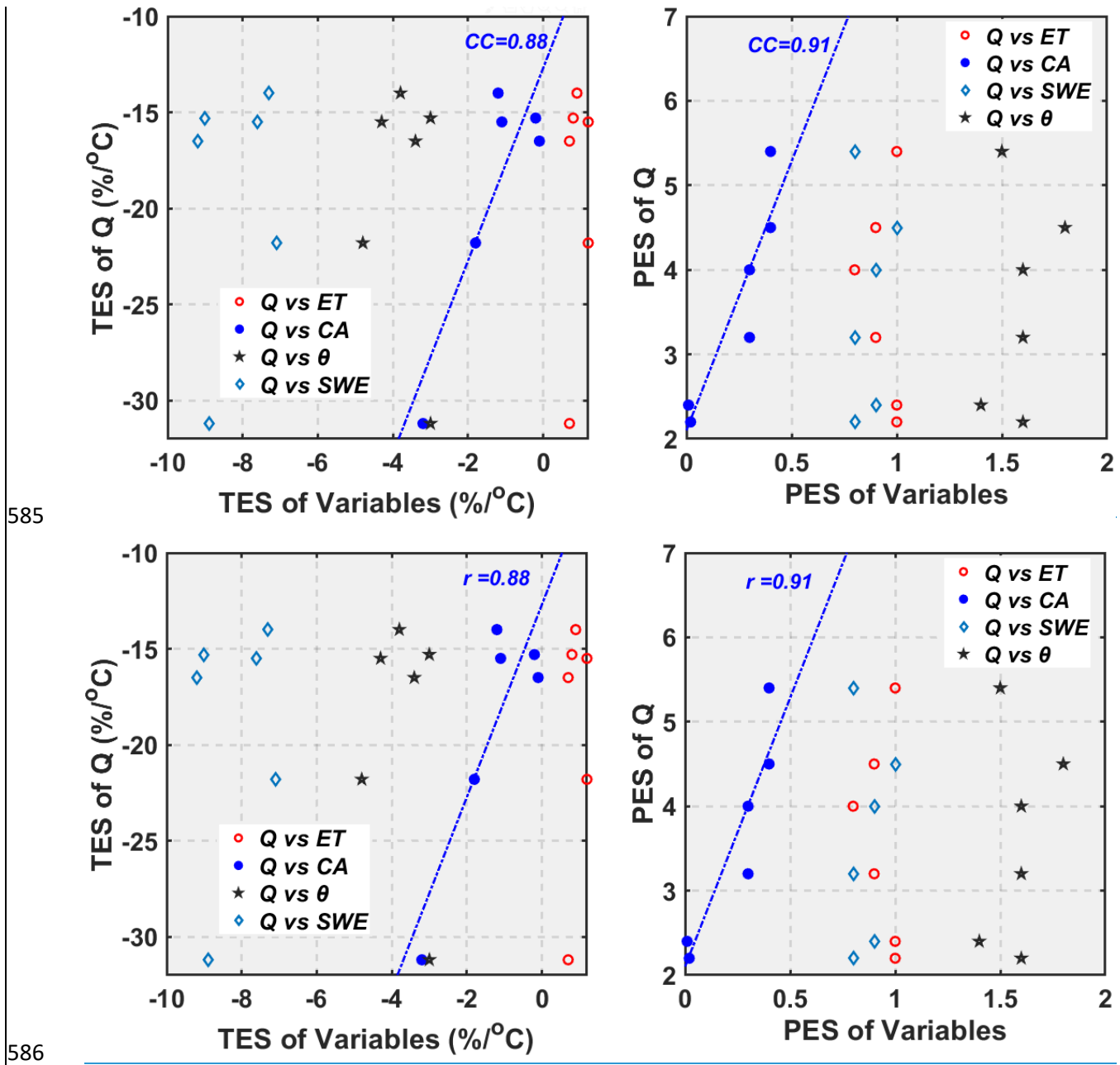
558 ~~Absolute mean~~ Mean absolute *TES* and *PES* of streamflow were much larger than those of snow
 559 and soil moisture (Table 6). Mean annual streamflow in the IG class was the most *T* sensitive at $-31.2\% \text{ } ^\circ\text{C}^{-1}$
 560 ¹. The SM class showed the smallest (absolute) *TES* for streamflow at $-6.0\% \text{ } ^\circ\text{C}^{-1}$. Streamflow *TES*
 561 ~~(absolute)~~ in the remaining classes were typically around $-17\% \text{ } ^\circ\text{C}^{-1}$. Similarly, IG had the largest
 562 streamflow *PES* of 5.4, followed by PHT with a *PES* of 4.5. Streamflow in SM showed comparable *PES* to
 563 that in MRV and PGL, whilst HEG and SI had the smallest *PES* of ≈ 2.3 .

564 Table 6. Mean elasticities of streamflow, ET, depressional storage (SD), and maximum connected area
 565 (CA) to ~~*T* and *P*~~ climate perturbations derived from the 35 climate input scenarios.

<u><i>TES</i> ($\% \text{ } ^\circ\text{C}^{-1}$)</u>	HEG	IG	SI	PGL	PHT	MRV	SM
<u><i>T</i> elasticity (<i>TES</i>, $\% \text{ } ^\circ\text{C}^{-1}$)</u>							
Annual streamflow	-16.5	-31.2	-15.3	-14.0	-21.8	-15.5	-6.0
Annual ET	0.7	0.7	0.8	0.9	1.2	1.2	2.1
Annual mean SD	-7.5	-10.2	-6.8	-5.5	-15.6	-2.9	0.1
Annual maximum CA	-0.1	-3.2	-0.2	-1.2	-1.8	-1.1	0.0
<u><i>P</i> elasticity (<i>PES</i>-)</u>							
Annual streamflow	2.4	5.4	2.2	3.2	4.5	4.0	3.6
Annual ET	1.0	1.0	1.0	0.9	0.9	0.8	0.4
Annual mean SD	1.5	1.5	1.3	1.3	3.0	1.2	2.7
Annual maximum CA	0.01	0.4	0.02	0.3	0.4	0.3	0.0

566 Apart from snowmelt contributions, streamflow in Prairie basins is controlled by ET and CA, the
 567 latter of which is determined by the state of SD which is most often filled by spring snowmelt. ET increased
 568 with both warming and *P* rising, as shown by its positive *TES* and *PES* (Table 6). The *TES* of ET was
 569 highest in the wetter and cropland-dominated classes, whilst *PES* of ET was highest in the grassland-
 570 characterized classes, because ET in the drier and grassland-characterized classes was more strongly limited
 571 by water availability but more limited by energy input in the wet and cropland-dominated classes. Therefore,
 572 *PES* of ET were around 1.0 in the grassland-characterized classes but lower than 1.0 in the cropland-
 573 dominated classes, especially in the SM basins. Basin-average SD in PHT showed the largest mean *TES*
 574 and *PES* among the basin types, partly because of its largest depressional storage capacity (Table 1). CA
 575 over the Prairies showed less sensitivity to *P* changes than ET, indicated by the *PES* values of only 0.01–
 576 ≈ 0.4 , which means the *P* input scenarios were not able to strongly change the fill-spill patterns of large
 577 depressions in the Prairies; whilst CA in classes of IG, PGL, PHT, and MRV showed visible sensitivity to

578 *T* change with absolute *TES* values comparable to that of *ET*, which can be explained by the fact that
 579 enhanced *ET* by warming strongly reduced *SD* in small wetland *HRUs* and their connectivity to the basin
 580 outlet. The *CA* in the *SM* class showed no sensitivity to *P* and *T* perturbations because all upper *HRUs*
 581 were connected to the channel in this class (see Figure 2b). These show that the climate sensitivity of *ET*,
 582 basin water storage and connectivity is greatly exceeded by that of streamflow generation. This is to be
 583 expected in a semi-arid to sub-humid climate where streamflow is intermittent and small in the baseline
 584 scenario.



587 Figure 9. Correlations between climate elasticities of annual streamflow (Q) and other variables in the
 588 basin types except SM. r means the Pearson correlation coefficient, and θ means the basin-average
 589 total soil moisture.

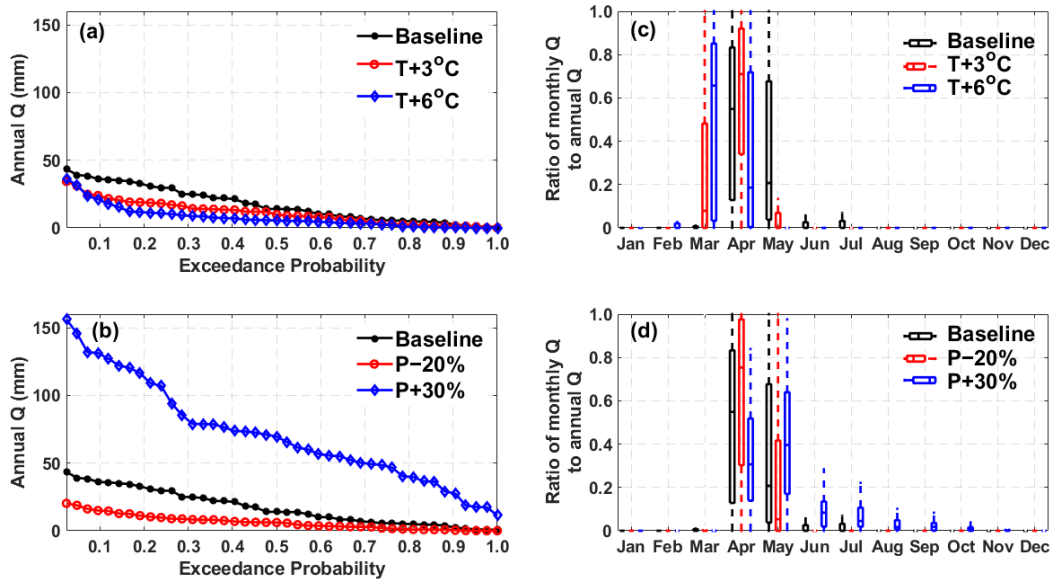
590 Correlation Coefficient (r) between the climate elasticities of annual streamflow
 591 and other hydrological variables indicated that the responses of annual streamflow to climate were mainly
 592 related to the response of CA in the wetland-characterized basins of HEG, IG, SI, PGL, PHT and MRV
 593 (Figure 9). The SM class was not included in this analysis because of its high connectivity. Climate
 594 elasticities of annual streamflow in SM should be mainly controlled by ET. r between TES of annual
 595 streamflow and CA was as high as 0.88, and that for PES was 0.91. Correlations between the climate
 596 elasticities of annual streamflow and other variables including ET, SWE, and basin-average soil moisture
 597 were typically lower and not significant (at the 5% level). For example, PES of ET and SWE showed small
 598 variations among the basin types, which differed from the considerable variations of streamflow PES .

599 Table 7. Required P increases (%) to offset the effects of warming ΔT and required warming degrees ($^{\circ}C$)
 600 to offset ΔP on annual streamflow (Q), and the maximum increase and decrease
 601 (percentage/magnitude) in mean annual streamflow forced by the 35 combined P/T perturbation
 602 scenarios.

	<u>HEG</u>	<u>IG</u>	<u>SI</u>	<u>PGL</u>	<u>PHT</u>	<u>MRV</u>	<u>SM</u>
Warming scenario	Required P increases (%) to offset warming ($^{\circ}C$)						
T +1 $^{\circ}C$	+5	+4.0	+3.8	+1.4	+2.4	-1.5	+1.5
T +2 $^{\circ}C$	+12.4	+7.7	+10.2	+5.6	+4.1	-1.0	+3.5
T +3 $^{\circ}C$	+19.4	+14.2	+18.8	+8.4	+9.1	+3.2	+4.8
T +4 $^{\circ}C$	+25.9	+15.7	+23.9	+13.1	+13.8	+6.7	+6.3
T +5 $^{\circ}C$	>+30	+17.8	+27	+15.9	+17.9	+12.4	+7.9
T +6 $^{\circ}C$	>+30	+27.7	>+30	+22.0	+23.5	+18.3	+9.1
P change scenario	Required ΔT (warming degrees ($^{\circ}C$)) to offset ΔP changes						
P -20%	NA	NA	NA	NA	NA	NA	NA
P +10%	+1.6	+2.32	+1.98	+3.3	+3.14	+4.56	>+6
P +20%	+3.12	+5.16	+3.26	+5.7	+5.38	>+6	>+6
P +30%	+4.65	>+6	+5.3	>+6	>+6	>+6	>+6
Maximum increase in annual <u>streamflow</u> (%/mm)	127/11	483/12	118/10	185/16	319/54	234/55	140/150
Maximum decrease in annual	-91/-8	-98/-2	-92/-8	-78/-7	-81/-14	-85/-20	-73/-78

streamflow Q
(%/mm)

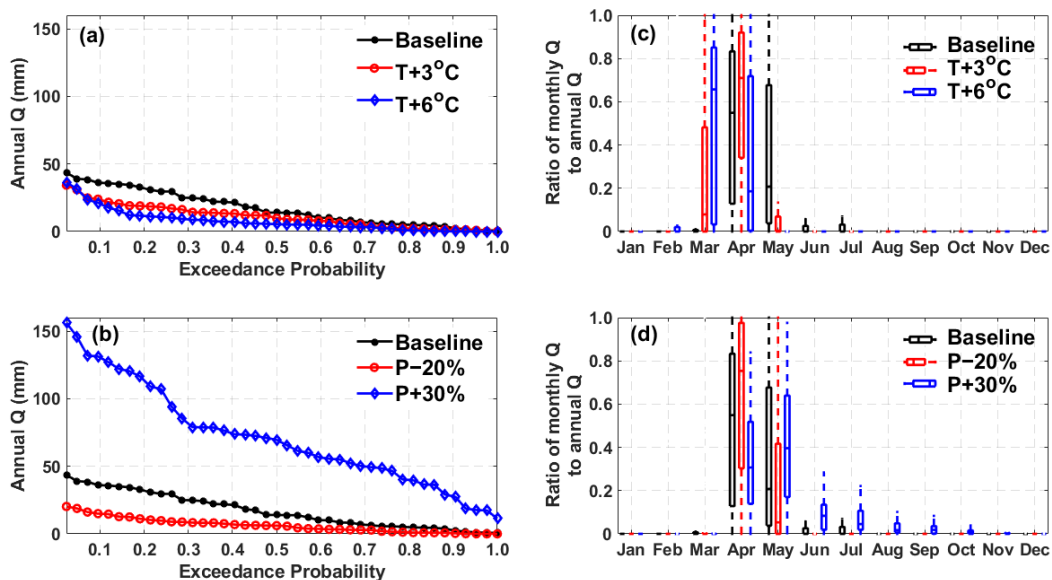
603 The effectiveness of increasing P in compensating for decreases in mean annual streamflow caused
604 by warming increased from the grassland-characterized classes to the cropland-dominated classes (Table
605 7). For example, around a 20% increase in P was required to offset the effects of warming by 3 °C in HEG,
606 whilst in SM, only up to 5% increase in P was required. Meanwhile, effects of the maximum warming of
607 6 °C can be fully offset by P increases up to 30% in PGL, PHT, MRV, and SM, whilst 30% increases in P
608 could only offset the effects of warming of 4–5 °C in HEG and SI. As expected, higher levels of warming
609 were required to offset the effects of the same P increases in the cropland-dominated classes. The maximum
610 warming of 6 °C can only offset the effects of P increase of up to 20% in the cropland-dominated classes
611 but can fully offset the effects of the maximum increase of 30% in the HEG and SI classes. The maximum
612 increases in mean annual streamflow forced by the 35 combined P and T scenarios ranged from 118% to
613 483% and 10 mm to 150 mm, whilst the maximum decreases ranged from –73% to –98% and –2
614 mm to –78mm–78 mm.



615
616 Figure 10. Changes in flow duration curve of annual streamflow (Q) during the modelling period (1965 –
617 2006) and the ratio of monthly Q to annual Q under T and P perturbation scenarios in the PHT class.
618 Boxplots refer to the inter-annual variability during the modelling period.

619 In addition to the long-term mean annual streamflow, T and P changes showed different impacts
620 on extremestatistically high and low annual streamflow during the modelingmodelling period. Taking the
621 PHT class as an example, warming caused larger magnitude reductions in annual streamflow with
622 exceedance probability of 0.1–0.4 than those in peak and extremely low annual streamflow (Figure 10a);

623 whilst P changes resulted in larger changes in peak annual streamflow (Figure 10b). Compared to maximum
 624 warming of 6°C , the maximum 30% increase in P caused greater increases not only in extreme peak and
 625 low annual streamflow but also in those with exceedance probability of $0.1\text{--}0.4$. The ratio of monthly
 626 streamflow to annual streamflow showed considerable switches under T and P perturbation scenarios. With
 627 warming of $3\text{--}6^{\circ}\text{C}$, the dominant period of monthly streamflow on annual streamflow switched from
 628 April-May to March-April (Figure 10c). Under 6°C warming, streamflow in March became the major
 629 contributor to annual streamflow, whilst that in May became very small. In contrast, streamflow in April-
 630 May will remain dominant on annual streamflow within the P change changes range from $\text{--}20\%$ to $+30\%$
 631 (Figure 10d). The P changes won't increase the contribution of March streamflow to annual streamflow,
 632 whilst dry scenario ($P\text{--}20\%$) considerably enhanced the contribution of April. In the wet scenario
 633 ($P+30\%$), contributions from streamflow in June, July, August and September to annual streamflow will
 634 be more visible.



635
 636 Figure 10. Changes in flow duration curve of annual streamflow (Q) during the modeling period (1965–
 637 2005) and the ratio of monthly Q to annual Q under T and P perturbation scenarios in the PHT class.
 638 Boxplots refer to the inter-annual variability during the modeling period.

639 5. Discussion

640 5.1 Basin hydrological sensitivity to climate changes

641 These modelingmodelling results are consistent with previous studies that focused on the impacts
 642 of warming (e. g., St-Jacques et al., 2018; Tanzeeba and Gan, 2012), which indicate earlier spring runoff,
 643 decreased mean annual streamflow and lower peak SWE in the Prairies. Johnson and Poiani (2016) found
 644 that a 20% increase in P could strongly offset the effects of 3°C warming on the wetland water storage in
 645 the Prairie Pothole Region, which is similar to the findings here of the combined effects of P and T in the

646 PGL and PHT classes (Table 3). Results from the Bad Lake basin in southwestern Saskatchewan (Fang and
647 Pomeroy, 2007) indicated that spring streamflow would decrease by 20% if air temperature increased by
648 1°C, and decrease by 1.6% in response to 1% decrease in precipitation, which is rather close to the findings
649 for the HEG and SI [classes](#) (in which Bad Lake basin lies) [classes](#) (Table 6). In this study we also showed
650 that annual streamflow showed a larger *PES* than did SWE, which is consistent with behaviour of Canadian
651 mountain basins to the west of our study region (Rasouli et al. 2022). However, the absolute *TES* of
652 streamflow over all the Prairie classes were larger than that of peak SWE, which is different from the
653 findings of Rasouli et al. (2022). Reasons for this can be that streamflow in the Prairies are typically
654 dominated by snowmelt in spring with small contribution from rainfall in spring and summer (Valeo et al,
655 2007; Pomeroy et al. 2010; 2014), but rainfall can be more important to streamflow generation in steeper
656 mountain basins. Moreover, the connectivity of the wetland complex to basin outlet is important to
657 streamflow generation in the Prairies and connectivity can be strongly regulated by ET which is enhanced
658 by warming.

659 [The *TES* and *PES* showed distinct gradients from drier to wetter climates over the Prairies as the](#)
660 [lower baseline SWE or annual streamflow in the drier and grassland-characterized classes \(Borchert, 1950;](#)
661 [Millett et al. 2009; Pomeroy et al. 2010\) likely resulted in higher percentage change of response variables](#)
662 [assessed herein \(Eqs. 2–3\). Whitfield et al. \(2020\) analyzed the changing trends in the Prairies streamflow](#)
663 [during 1920-2015 and demonstrated that streams in the southwestern Canadian Prairies are shifting to drier](#)
664 [conditions, and that the northeast is getting wetter. The modelling results here align with their findings and](#)
665 [partly reveal the underlying mechanisms: streamflow in the western HEG class and southern SI class](#)
666 [declined more rapidly with warming but increased more slowly with elevated *P* than those in the eastern](#)
667 [SM class and the northern MRV class. Meanwhile, streamflow reduction in the eastern basins due to](#)
668 [warming is more easily offset by *P* increase than in the western basins. Forced by future warming,](#)
669 [streamflow in the drier and grassland-characterized basins will probably continue to get drier, and wetter](#)
670 [cropland-dominated basins will continue to get wetter.](#)

671 [In addition to the climate difference, landscape traits among the basins also contributed to the varied](#)
672 [hydrological sensitivities. For example, the SM class was characterized by fewer isolated wetlands and](#)
673 [higher connectivity than the other classes, which resulted in smaller streamflow sensitivity to warming. The](#)
674 [non-effective fraction in IG was much larger than that in SI, and when forced by the same meteorological](#)
675 [observations at Swift Current, streamflow in IG showed much larger sensitivities to *T* and *P* perturbations.](#)
676 [Wetland fraction and depressional storage capacity in PHT is larger than that in MRV. When forced by](#)
677 [similar climate at Yorkton and Brandon respectively, streamflow, ET and CA in PHT showed larger](#)
678 [sensitivities. This can be explained by hydrological connectivity and streamflow generation in the PHT](#)
679 [basins being more limited by water availability because of the larger depressional storage capacity.](#)

680 [However, the influence of landscape traits on sensitivity of basin-average snow to climate perturbations](#)
681 [was smaller than the influence of site climate.](#)

682 To reduce the computational effort and conduct hydrological ~~modeling~~modelling forced by 35
683 climate input scenarios in all the seven basin types, one representative AHCCD station was selected as an
684 exemplar for each of the basin types. ~~This is one of the limitations in this study, as the hydrological~~
685 ~~sensitivities associated with different baseline climates were not compared for the same basin class.~~ Spence
686 et al. (2022a) indicated that sensitivity to climate perturbation varied with local climate within the same
687 Prairie basin class. The elasticity ~~modeling~~modelling here also demonstrated dynamic percentage changes
688 in peak SWE with warming and per % *P* increase under different *P* and *T* input scenarios (Figure 5). Mean
689 *TES* and *PES* used in this study were calculated as the average change rate in hydrological variables forced
690 by the 35 climate inputs at the representative AHCCD stations, which ~~are~~were therefore reasonably used
691 as the hydrological sensitivity assessment for the typical locations in each of the classes. In Spence et al.
692 (2022a), simulating streamflow in HEG with a Medicine Hat climate resulted in an absolute *TES* 3.3-% °C⁻¹
693 ¹ higher than with a Brandon climate. In this study, when forcing the HEG VB model at Medicine Hat and
694 the MRV VB model at Brandon, the *TES* difference for annual streamflow ~~is~~was as small as 1.0-% °C⁻¹
695 (Table 6). This suggests simulating streamflow in one basin class with a representative climate likely
696 reduces uncertainty in the sensitivity assessment than running a VB model with a distant unrepresentative
697 meteorology.

698 ~~*TES* and *PES* showed distinct gradients from drier to wetter climates over the Prairies as the lower~~
699 ~~baseline SWE or annual streamflow in the drier and grassland characterized classes (Borchert, 1950; Millett~~
700 ~~et al. 2009; Pomeroy et al. 2010) likely resulted in higher percentage change of response variables assessed~~
701 ~~herein (Eqs. 1 – 2). Whitfield et al. (2020) analyzed the changing trends in the Prairies streamflow during~~
702 ~~1920–2015 and demonstrated that streams in the southwestern Canadian Prairies are shifting to drier~~
703 ~~conditions, and that the northeast is getting wetter. The modeling results here align with their findings and~~
704 ~~partly reveal the underlying mechanisms: streamflow in the western HEG class and southern SI class~~
705 ~~declined more rapidly with warming but increased more slowly with *P* rising than those in the eastern SM~~
706 ~~class and the northern MRV class. Meanwhile, streamflow reduction in the eastern basins due to warming~~
707 ~~is more easily offset by *P* increase than in the western basins. Forced by future warming, streamflow in the~~
708 ~~drier and grassland characterized basins will probably continue to get drier, and wetter cropland dominated~~
709 ~~basins will continue to get wetter.~~

710 In addition to the climate difference, landscape traits among the basins also contributed to the varied
711 hydrological sensitivities. For example, the SM class was characterized by fewer wetlands and higher
712 connectivity than the other classes, which resulted in smaller streamflow sensitivity to warming. The non-
713 effective fraction in IG was much larger than that in SI, and when forced by the same meteorological

714 observations at Swift Current, streamflow in IG showed much larger sensitivities to T and P perturbations.
715 Wetland fraction and depressional storage capacity in PHT is larger than that in MRV. When forced by
716 similar climate at Yorkton and Brandon, streamflow, ET and CA in PHT showed larger sensitivities. This
717 can be explained by hydrological connectivity and streamflow generation in the PHT basins being more
718 limited by water availability because of the larger depressional storage capacity. However, the influence of
719 landscape traits on sensitivity of basin-average snow to climate perturbations was smaller than the influence
720 of site climate.

721 5.2 Implications for adaptive water management strategies

722 Considering risks to freshwater availability caused by economic and population growth and
723 agricultural expansion in the Prairies concomitant with climate change (St-Jacques et al., 2018), these
724 scenario-based modelling results have important implications for the development of adaptive strategies to
725 changing climate for the Prairie Provinces. The sensitivity analysis based on a physically based hydrological
726 model provides a diagnosis of the underlying processes behind regional hydrological response to climate
727 change, and provides insightful information to support the design and direction of adaptive practices
728 (Tarnoczi, 2011). Separation of P and T sensitivity could serve as guidance for adaptation strategies in
729 response to short-term hydrological flooding triggered by P events, and long-term warming and droughts
730 caused by decadal T increases (Zhang et al., 2021). Calculating elasticity of hydrological processes under
731 variable climate and basin types over the Prairie provides useful information for how these processes may
732 change and how hydrological sensitivity to climate perturbations can differ, across the spectrum of climate
733 conditions and landscapes (Wheater and Gober, 2013). The sensitivity assessment indicated to what extent
734 snow processes, soil moisture and streamflow will be significantly impacted by meteorological forcing
735 changes in the different basins spanning the region, delivering informative knowledge for potential
736 management of agricultural activities. The combined effects of P and T perturbations on soil moisture and
737 streamflow have implications for the Prairie Provinces' climate change plans that are aimed at building
738 climate resilience (Sauchyn et al., 2017), including improving understanding of future hydrology changes
739 and the quantitative examinations of the tradeoff between P increase and warming, which importantly differ
740 according to basin type and climate in the study region.

741 Comparisons among the land covers and basin types suggested that both basin characteristics and
742 local climate influenced the basin hydrological sensitivities. The lower P effectiveness in compensating for
743 warming effects in the drier and grassland-characterized basins highlighted their tendency to undergo more
744 drying than the wetter and cropland-dominated basins which are historically wetter. Adaptation strategies
745 in the drier basins should be carefully designed for a future where surface water is scarcer. In the wetter
746 basins concentrated in eastern parts of the study region, it seems the ability to cope with more water in
747 many years will be necessary in the short term, but long-term drying is also possible.

5.3 Uncertainty and limitations

High uncertainty in ~~modeled~~modelled sensitivities in the Prairies has been documented before (Unduche et al., 2018). Sources of uncertainty in this study include those ~~with VB model parameter estimation, from~~ inaccurate meteorological data ~~from observations at the AHCCD station and the stations,~~ use of perturbed climate scenarios, and model process representation and parameterization associated with a VB approach.

~~There is uncertainty in the meteorological measurements at the AHCCD stations, particularly for severe summer rainstorms. The misrepresentations of the intensity and occurrence of such events in the P inputs would lead to an underestimation of simulated streamflow in the warm seasons across the Prairies.~~ The 35 perturbed climate scenarios were set up based on a delta approach with the assumption that P and T perturb linearly without considering the seasonal dynamics. ~~Despite that, the delta approach facilitates the investigation of climate sensitivity based on a long term simulation and has been acceptably used to represent the uncertainty in the~~The linear approach thus did not consider disproportionate changes in extreme precipitation events. Seasonal patterns of P and T in the perturbed scenarios are the same as in the baseline scenario observed at the AHCCD stations. This approach was used because the focus of our study is a sensitivity analysis of snowmelt, soil moisture and streamflow in response to potential future climate perturbations, rather than a modelling projection of future hydrology under future climates. Delta perturbations have successfully represented the uncertainty in projected future climate over the Prairies (Zhang et al. 2021). The maximum warming of 6 °C, and the future change range in P of ~~-20% to +30%~~ were derived from Canada's Changing Climate report edited by Bush and Lemmen (2019) and projections by Jiang et al. (2017), and are close to the delta changes downscaled from a couple of GCMs in Forbes et al. (2011). However, caution should be taken when extrapolating or interpolating these results to the specific basins, as the modeling used VBs that represent the typical hydrological characteristics of a basin type in a hydroclimatic region of the Canadian Prairies. ~~-20% to +30%~~ are within the realm of projections (Bush and Lemmen, 2019; Jiang et al. 2017; Forbes et al. 2011). Characterized by increment changes in T (i.e., per degree) and P (i.e., per 10%), the perturbed climate scenarios are not only suitable for the assessment of hydrological sensitivity (i.e., changes in hydrological variables caused by per degree warming or per 10% increases in P) but also able to examine to what extent the impact of warming can be compensated for by P changes. Despite the limitations, the delta approach has been shown to provide reasonable temporal distributions of extreme dry, wet, hot and cold climate conditions documented in long-term historical observations (He et al. 2021). This allows the model calculation of shifts from spring snowfall to spring rainfall with increasing T , which is associated with the generation of extreme flow. Inter-annual variability, particularly with anticipated new precipitation extremes warrants further consideration, as to include additional analysis of this regard herein would be unwieldy.

782 All surface hydrological processes in CRHM are physically represented (Pomeroy et al. 2013;
783 2022). Because of this, most model parameters (which have physical meaning) are observable, and do not
784 require calibration. Some deeper sub-surface processes, however, are represented conceptually in CRHM
785 and therefore the parameters (which are not normally observed in any case) might require calibration. But
786 this was not done in the models presented here as the parameters, which were abducted from previous
787 studies in similar basins, did well enough to yield good agreement in our model assessment stages. First,
788 this is because sub-surface flows are typically unimportant runoff generation mechanisms in the Canadian
789 Prairies. Second, the CRHM-based virtual basin hydrological models were not specifically tailored to site-
790 specific basins. Instead, they were designed to represent the median land cover and hydrological
791 characteristics of each of the seven basin types. Therefore, calibrating model parameters using those from
792 specific basins would have biased the results away from the typical basin of each class. The approach of
793 using parameters from previous studies was taken to avoid using optimized parameters that may yield high
794 performance in the calibrated basins but perform poorly in other ungauged basins of the same class.
795 Additionally, it is important to note that streamflow discharge observations over the Canadian Prairies are
796 very limited, especially for small basins, making it difficult to calibrate the CRHM-based models at each
797 specific location within the Prairie basins. The ability of CRHM to give good results without calibration
798 has been well established in the published literature. Pomeroy et al (2022) summarizes many examples of
799 this. The use of CRHM parameters “abducted” from similar basins has also been established in Pomeroy et
800 al. (2013). Therefore, while there is inherent uncertainty in the model (He and Pomeroy, 2023), parameter
801 uncertainty should have limited influence on the modelling assessment in this study.

802 Virtual basins (VB) were used to represent the typical hydrological behaviour in each of the seven
803 basin types. The CRHM-based VB hydrological models were structured and parameterized using the
804 median characteristics of each class. The VB models were then utilized to assess the median sensitivity of
805 hydrological processes to climate perturbations based on representative meteorological data. Therefore,
806 simulations will inevitably show biases from the gauged streamflow due to the virtual basin nature of the
807 models. Further, this analysis does not represent the full range of hydrological variability within each basin
808 class which is one limitation of the regional approach favoured here. Despite these considerations, there is
809 reasonable agreement between the simulated and observed seasonal pattern of streamflow based on
810 graphical assessment. This approach enabled comparisons of the general response of hydrological processes
811 amongst these basin types. However, cautions should be taken when interpreting these assessments to real
812 basins in the Prairies. The results are meant to reflect a regional response, rather than that in any specific
813 location. ~~Finally, using the delta method does not allow for an assessment of hydrological sensitivity to~~
814 ~~specific or ensemble projections of climate changes in the region. Specifically local land cover, hydrography~~
815 ~~and soil properties would be taken into account for the assessment of how they may alter estimates from~~

816 those presented here in a physical basin. Moreover, changes in land cover and soil parameters under
817 perturbed climate were not considered (see Spence et al. 2022b for such an example). The modelling
818 outcomes cannot be interpreted as future hydrological projections in real basins.

819 **5.2 Implications for adaptive water management strategies**

820 ~~Considering the freshwater availability risk caused by economic and population growth and~~
821 ~~agricultural expansion in the Prairies concomitant with climate change (St Jacques et al., 2018), these~~
822 ~~scenario-based modeling results have important implications for the development of adaptive strategies to~~
823 ~~changing climate for the Prairie Provinces. The sensitivity analysis based on a physically based hydrological~~
824 ~~model provides a diagnosis of the underlying processes behind hydrological response to climate change,~~
825 ~~and provides insightful information to support the design and direction of adaptive practices (Tarnoezi,~~
826 ~~2011). Separation of P and T sensitivity could serve as guidance for adaptation strategies in response to~~
827 ~~short-term hydrological flooding triggered by precipitation events, and long-term warming and droughts~~
828 ~~caused by decadal temperature increases (Zhang et al., 2021). Elasticity modeling of hydrological processes~~
829 ~~under variable climate and basin types over the Prairie provides useful information for how hydrological~~
830 ~~processes and streamflow may change and how the hydrological sensitivity to climate perturbations can~~
831 ~~differ, across the spectrum of climate and landscapes (Wheater and Gober, 2013). The sensitivity~~
832 ~~assessment indicated to what extent snow processes, soil moisture and streamflow will be significantly~~
833 ~~impacted by meteorological forcing changes in the different regions, delivering informative knowledge for~~
834 ~~potential management of agricultural activities. The combined effects of P and T perturbations on soil~~
835 ~~moisture and streamflow have implications for the Prairie Provinces' climate change plans that are aimed~~
836 ~~at building climate resilience (Sauchyn et al., 2017), including improving understanding of future hydrology~~
837 ~~changes and the quantitative examinations of the tradeoff between P increase and warming, which~~
838 ~~importantly differ according to basin type and climate in the study region.~~

839 **8.6. Conclusions**

840 This study evaluated hydrological sensitivity to climate across the Canadian Prairies based on a
841 basin-classification and virtual basin (VB) ~~modeling~~modelling approach, with different land covers
842 represented with HRUs. Among the different land covers, snow accumulation in wetlands is more sensitive
843 to climate perturbations than that in cropland and grassland. Peak SWE in cropland showed larger climate
844 sensitivity than that in grassland in wet and cropland-dominated basin types (PGL, PHT, MRV and SM),
845 but was less sensitive in the dry and grassland-characterized basin types (HEG, IG, and SI). Wetland soil
846 moisture was more sensitive to warming than that in cropland and grassland, with cropland soil moisture
847 being the least sensitive to temperature ~~(T)~~. Precipitation ~~(P)~~ sensitivity for soil moisture in cropland,
848 grassland and wetland tended to be consistent over the Prairies. Due to the joint influences of land cover
849 and site climate, snow accumulation and melt runoff at the basin scale were more sensitive to warming in

850 the drier and grassland-characterized basins than in the wetter and cropland-dominated basins. Basin-
851 average soil moisture was more sensitive to T and P perturbations in basins typified by pothole depressions
852 and broad river valleys than that in grassland-characterized basins. Annual streamflow exhibited the
853 greatest sensitivities to T and P in the dry and poorly connected IG basins but the smallest sensitivity to T
854 in the wet and well-connected SM basins. The effectiveness of P increases in compensating for the effects
855 of warming on snow accumulation and annual streamflow was higher in wet than in dry basins. For snow
856 accumulation, the maximum 30% increase in P could fully offset warming of 3 °C in wet SM, but could
857 only compensate for 2 °C in the dry and grassland-characterized basins (e.g. HEG). For annual streamflow,
858 the maximum P increase of 30% could offset decreases caused by warming of 6 °C in the wetter and
859 cropland-dominated basins in the eastern prairies, but could not in the drier grassland-characterized basins
860 of the western prairies.

861 These sensitivity analyses improved understanding of variations in hydrological responses to
862 climate change over the Canadian Prairies, highlighting where important hydrological states for agricultural
863 productivity (e.g. soil moisture) are sensitive and likely to change due to overwhelming effects of warming,
864 even where potential P increases occur. Assessments of the sensitivities of snow processes, soil moisture,
865 ET, and connected area provide diagnosis of the underlying processes behind streamflow response to
866 climate change over the Prairies. ~~Both basin characteristics and local climate played influences on the basin~~
867 ~~hydrological sensitivities. The lower P effectiveness in compensating for warming effects in the drier and~~
868 ~~grassland characterized basins highlighted their tendency to undergo more drying than the wetter and~~
869 ~~cropland dominated basins which are historically wetter. Inter annual variability, particularly with~~
870 ~~anticipated new precipitation extremes, has not been considered here, and warrants further consideration.~~
871 ~~Adaptation strategies in the drier basins should be carefully designed for a future where surface water is~~
872 ~~scarcer. In the wetter basins concentrated in eastern parts of the study region, it seems the ability to cope~~
873 ~~with more water in many years will be necessary in the short term, but long term drying is also possible.~~

875 **Acknowledgements**

876 The authors wish to acknowledge funding provided by the Canada First Research Excellence Fund to
877 Global Water Futures that supported this research. Additional support from the Canada Research Chairs,
878 and Natural Sciences and Engineering Research Council of Canada is gratefully acknowledged. The role
879 of Mr. Tom Brown in developing and supporting the CRHM Platform in his 50-year hydrological modelling
880 career at the University of Saskatchewan and the research findings of the Division of Hydrology and Centre
881 for Hydrology at the same university were crucial to this research.

882

883 **References**

- 884 Anteau, M. J., Wiltermuth, M. T., van der Burg, M. P., and Pearse, A.T.: Prerequisites for Understanding
885 Climate-Change Impacts on Northern Prairie Wetlands, *Wetlands*, 36, 299–307,
886 <https://doi.org/10.1007/s13157-016-0811-2>, 2016.
- 887 Armstrong, R. N., Pomeroy, J. W., and Martz, L. W.: Estimating evaporation in a Prairie landscape under
888 drought conditions, *Canadian Water Resour. J.*, 35, 173– 186, 2010.
- 889 Armstrong, R. N., Pomeroy, J. W., and Martz, L. W.: Variability in evaporation across the Canadian Prairie
890 region during drought and non-drought periods, *J. Hydrol.*, 521, 182–195,
891 <https://doi.org/10.1016/j.jhydrol.2014.11.070>, 2015.
- 892 Borchert, J. R.: The climate of the central north American grassland, *Ann. Assoc. Am. Geogr.*, 40, 1–39.,
893 <https://doi.org/10.1080/00045605009352020>, 1950.
- 894 Bush, E. and Lemmen, D. S.: Canada’s Changing Climate Report, Government of Canada, Ottawa, ON.,
895 <https://changingclimate.ca/CCCR2019>, 2019.
- 896 Coles, A. E., McDonnell, J., and McConkey, B. G.: Fifty Years of Recorded Hillslope Runoff on Seasonally
897 Frozen Ground: The Swift Current, Saskatchewan, Canada, Dataset, *Earth Syst. Sci. Data.*, 11 (3),
898 1375–83, <https://doi.org/10.5194/essd-11-1375-2019>, 2019.
- 899 Cordeiro, M. R. C., Wilson, H. F., Vanrobaeys, J., Pomeroy, J. W., and Fang, X.: Simulating cold-region
900 hydrology in an intensively drained agricultural watershed in Manitoba, Canada, using the Cold
901 Regions Hydrological Model, *Hydrol. Earth Syst. Sci.*, 21(7), 3483–3506, doi:10.5194/hess-21-
902 3483-2017, 2017.
- 903 Cordeiro M. R. C., Liang K., Wilson H. F., Vanrobaeys J., Lobb D. A., Fang, X., and Pomeroy, J. W.:
904 Simulating the hydrological impacts of land use conversion from annual crop to perennial forage
905 in the Canadian Prairies using the Cold Regions Hydrological Modelling platform, *Hydrol. Earth
906 Syst. Sci.*, 26, (2022), 5917:5931, doi: 10.5194/hess-26-5917-2022, 2022.
- 907 Costa, D., Shook, K., Spence, C., Elliott, J., Baulch, H., Wilson, H., and Pomeroy, J. W.: Predicting Variable

908 Contributing Areas, Hydrological Connectivity, and Solute Transport Pathways for a Canadian
909 Prairie Basin, *Water Resour. Res.*, 56(12), doi:10.1029/2020WR027984, 2020.

910 Fang, X. and Pomeroy, J. W.: Snowmelt runoff sensitivity analysis to drought on the Canadian prairies,
911 *Hydrol. Process.*, 2274(21), 2594–2609, doi:10.1002/hyp, 2007.

912 Fang, X. and Pomeroy, J. W.: Modelling blowing snow redistribution to prairie wetlands, *Hydrol. Process.*,
913 23, 2557–2569, doi:10.1002/hyp.7348, 2009.

914 Fang, X., Pomeroy, J. W., Westbrook, C. J., Guo, X., Minke, A. G., and Brown, T.: Prediction of snowmelt
915 derived streamflow in a wetland dominated prairie basin, *Hydrol. Earth Syst. Sci.*, 14(6), 991–1006,
916 doi:10.5194/hess-14-991-2010, 2010.

917 Forbes, K. A., Kienzle, S. W., Coburn, C. A., and Byrne, J. M., Rasmussen, J.: Simulating the hydrological
918 response to predicted climate change on a watershed in southern Alberta, Canada, *Clim. Change*,
919 105, 555–576, <https://doi.org/10.1007/s10584-010-9890-x>, 2011.

920 Granger, R. J. and Gray, D. M.: A net radiation model for calculating daily snowmelt in open environments,
921 *Nordic Hydrology*, 21, 217 – 234, 1990.

922 Gray D. M.: *Handbook on the Principles of Hydrology*, Water Information Center, Inc. Port: Washington,
923 NY, 1970.

924 Gray, D. M., Toth, Brenda, Zhao, Litong, Pomeroy, J. W., and Granger, R. J.: Estimating areal snowmelt
925 infiltration into frozen soils, *Hydrol. Process.*, 15 (16), 3095–3111, 2001.

926 [He, Z. and Pomeroy, J. W.: Assessing hydrological sensitivity to future climate change in the Canadian](#)
927 [southern boreal forest, *J. Hydrol.* 624, 129897, 2023.](#)

928 [He, Z., Pomeroy, J. W., Fang, X., and Peterson, A.: Sensitivity analysis of hydrological processes to](#)
929 [perturbed climate in a southern boreal forest basin, *J. Hydrol.* 601, 126706, 2021.](#)

930 Jiang, R., Gan, T. Y., Xie, J., Wang, N., and Kuo, C.: Historical and potential changes of precipitation and
931 temperature of Alberta subjected to climate change impact: 1900–2100, *Theor. Appl. Climatol.*,
932 127:725–739, 2017.

933 Johnson, W. C. and Poiani, K. A.: Climate Change Effects on Prairie Pothole Wetlands: Findings from a
934 Twenty-five Year Numerical Modeling Project, *Wetlands*, 36, 273–285, doi:10.1007/s13157-016-
935 0790-3, 2016.

936 Johnson, W. C., Millett, B. V., Gilmanov, T., Voldseth, R. A., Guntenspergen, G. R., and Naugle, D. E.:
937 Vulnerability of northern prairie wetlands to climate change, *Bioscience*, 55(10), 863–872,
938 doi:10.1641/0006-3568(2005)055[0863:VONPWT]2.0.CO;2, 2005.

939 Kienzle, S. W., Nemeth, M. W., Byrne, J. M., and MacDonald, R. J.: Simulating the hydrological impacts
940 of climate change in the upper North Saskatchewan River basin, Alberta, Canada, *J. Hydrol.*, 412–
941 413, 76–89, doi:10.1016/j.jhydrol.2011.01.058, 2012.

942 Leibowitz, S. G. and Vining, K. C.: Temporal connectivity in a prairie pothole complex, *Wetlands*, 23(1),
943 13-25, 2003.

944 MacDonald, R. J., Byrne, J. M., Boon, S., and Kienzle, S. W.: Modelling the Potential Impacts of Climate
945 Change on Snowpack in the North Saskatchewan River Watershed, Alberta, *Water Resour. Manag.*,
946 26(11), 3053–3076, doi:10.1007/s11269-012-0016-2, 2012.

947 Mahmood, T. H., and Pomeroy, J. W., Wheeler, H. S., and Baulch, H. M.: Hydrological responses to
948 climatic variability in a cold agricultural region, *Hydrol. Process.*, 31(4), 854–870,
949 doi:10.1002/hyp.11064, 2017.

950 Mekis, É. and Vincent, L. A.: An overview of the second generation adjusted daily precipitation dataset for
951 trend analysis in Canada, *Atmos.- Ocean.*, 49, 163–177, 2011.

952 Millett, B., Johnson, W.C., and Guntenspergen, G.: Climate trends of the North American prairie pothole
953 region 1906-2000, *Clim. Change*, 93, 243–267, <https://doi.org/10.1007/s10584-008-9543-5>, 2009.

954 Muhammad, A., Evenson, G. R., Stadnyk, T. A., Boluwade, A., Jha, S. K., and Coulibaly, P.: Impact of
955 model structure on the accuracy of hydrological modeling of a Canadian Prairie watershed, *J.*
956 *Hydrol. Reg. Stud.*, 21, 40–56, doi:10.1016/j.ejrh.2018.11.005, 2019.

957 Pomeroy, J. W., Brown, T., Fang, X., Shook, K. R., Pradhananga, D., Armstrong, R., Harder, P., Marsh,
958 C., Costa, D., Krogh, S. A., Aubry-Wake, C., Annand, H., Lawford, P., He, Z., Kompanizare, M.,
959 and Lopez-Moreno, J. I.: The Cold Regions Hydro- logical Modelling Platform for hydrological
960 diagnosis and prediction based on process understanding, *J. Hydrol.*, 615, 128711,
961 <https://doi.org/10.1016/j.jhydrol.2022.128711>, 2022.

962 Pomeroy, J. W., Fang, X., Westbrook, C., Minke, A., Guo, X., and Brown, T.: Prairie Hydrological Model
963 Study Final Report, Cen- tre for Hydrol- ogy Report No. 7, University of Saskatchewan, Saskatoon,
964 113 pp., [https://research-groups.usask.ca/hydrology/ publications/reports.php](https://research-groups.usask.ca/hydrology/publications/reports.php), 2010.

965 Pomeroy, J., Fang, X., and Ellis, C.: Sensitivity of snowmelt hydrology in Marmot Creek, Alberta, to forest
966 cover disturbance, *Hydrol. Process*, 26, 1891–1904, 2012.

967 Pomeroy, J. W., Fang, X., Shook, K., and Whitfield, P. H.: Predicting in ungauged basins using physical
968 principles obtained using the deductive, inductive, and abductive reasoning approach, in: Pomeroy,
969 J.W., Spence, C., Whitfield, P.H. (Eds.), *Putting Prediction in Ungauged Basins into Practice*,
970 Canadian Water Resources Association, pp. 41–62, 2013.

971 Pomeroy, J. W., Gray, D. M., Brown, T., Hedstrom, N. R., Quinton, W., Granger, R. J., and Carey, S.: The
972 cold regions hydrological model: a platform for basing process representation and model structure
973 on physical evidence, *Hydrol. Process.*, 21, 2650–2667, 2007.

974 Pomeroy, J. W., Gray, D. M., Shook, K. R., Toth, B., Essery, R. L. H., Pietroniro, A., and Hedstrom, N.:
975 An evaluation of snow accumulation and ablation processes for land surface modelling, *Hydrol.*

976 Process., 12, 2339–2367, 1998.

977 Pomeroy, J. W., Gray, D. M., and Landine, P. G.: The Prairie Blowing Snow Model: characteristics,
978 validation, operation, *J. Hydrol.*, 144, 165–192, 1993.

979 Pomeroy, J. W., Shook, K., Fang, X., Dumanski, S., Westbrook, C., and Brown, T.: Improving and testing
980 the prairie hydrological model at Smith Creek Research Basin, Centre for Hydrology Report No.14.
981 May, 2014.

982 Rasouli, K., Pomeroy, J. W., and Whitfield, P. H.: Hydrological Responses of Headwater Basins to Monthly
983 Perturbed Climate in the North American Cordillera, *J. Hydrometeorol.*, 20, pp.863:882, doi:
984 10.1175/JHM-D-18-0166.1, 2019.

985 Rasouli, K., Pomeroy, J. W., and Whitfield, P. H.: The sensitivity of snow hydrology to changes in air
986 temperature and precipitation in three North American headwater basins, *J. Hydrol.*, 606, 127460,
987 doi: 10.1016/j.jhydrol.2022.127460, 2022.

988 Samuel, J., Coulibaly, P., and Kollat, J.: CRDEMO: Combined regionalization and dual entropy-
989 multiobjective optimization for hydrometric network design, *Water Resour. Res.*, 49, 8070–8089,
990 <https://doi.org/10.1002/2013WR014058>, 2013.

991 Sauchyn, D., Davidson, D., and Johnston, M.: Prairie Provinces; Chapter 4 in *Canada in a Changing Climate:
992 Regional Perspectives Report*, 2017.

993 Schaake, J. C.: From climate to flow. In: Waggoner, P.E. (Ed.), *Climate change and U.S. water resources*,
994 177–206, John Wiley and Sons Inc., New York, USA, 1990.

995 Shahabul Alam, M. and Elshorbagy, A.: Quantification of the climate change-induced variations in
996 Intensity-Duration-Frequency curves in the Canadian Prairies, *J. Hydrol.*, 527, 990–1005,
997 doi:10.1016/j.jhydrol.2015.05.059, 2015.

998 Shaw, D. A., Vanderkamp, G., Conly, F. M., Pietroniro, A., and Martz, L.: The Fill-Spill Hydrology of
999 Prairie Wetland Complexes during Drought and Deluge, *Hydrol. Process.*, 26, 3147–3156,
1000 <https://doi.org/10.1002/hyp.8390>, 2012.

1001 Shook, K., Pomeroy, J. W., Spence, C., and Boychuk, L.: Storage dynamics simulations in prairie wetland
1002 hydrology models: Evaluation and parameterization, *Hydrol. Process.*, 27(13), 1875–1889,
1003 doi:10.1002/hyp.9867, 2013.

1004 Shook, K., Pomeroy, J., and van der Kamp, G.: The transformation of frequency distributions of winter
1005 precipitation to spring streamflow probabilities in cold regions; case studies from the Canadian
1006 Prairies, *J. Hydrol.*, 521, 395–409, doi:10.1016/j.jhydrol.2014.12.014, 2015.

1007 Spence, C., He, Z., Shook, K., Mekonnen, B., Pomeroy, J., Whitfield, C., and Wolfe, J.: Assessing
1008 hydrological sensitivity of grassland basins in the Canadian Prairies to climate using a basin
1009 classification-based virtual modelling approach, *Hydrol. Earth Syst. Sci.*, 26, 1801-

1010 1819, <https://doi.org/10.5194/hess-26-1801-2022>, 2022a.

1011 Spence, C., He, Z., Shook, K., Pomeroy, J., Whitfield, C., and Wolfe, J.: Assessing runoff sensitivity of
1012 North American Prairie Pothole Region basins to wetland drainage using a basin classification-
1013 based virtual modelling approach, *Hydrol. Earth Syst. Sci.*, 26, 5555–5575,
1014 <https://doi.org/10.5194/hess-26-5555-2022>, 2022b.

1015 St-Jacques, J. M., Andreichuk, Y., Sauchyn, D. J., and Barrow, E.: Projecting Canadian Prairie Runoff for
1016 2041–2070 with North American Regional Climate Change Assessment Program (NARCCAP)
1017 Data, *J. Am. Water Resour. Assoc.*, 54(3), 660–675, doi:10.1111/1752- 1688.12642, 2018.

1018 Tanzeeba, S. and Gan, T. Y.: Potential impact of climate change on the water availability of South
1019 Saskatchewan River Basin, *Clim. Change*, 112(2), 355–386, doi:10.1007/s10584-011-0221-7,
1020 2012.

1021 Tarnoczi, T.: Transformative learning and adaptation to climate change in the Canadian Prairie agro-
1022 ecosystem, *Mitig. Adapt. Strateg. Glob. Chang.*, 16(4), 387–406, doi:10.1007/s11027-010-9265-7,
1023 2011

1024 Unduche, F., Tolossa, H., Senbeta, D., and Zhu, E.: Evaluation of four hydrological models for operational
1025 flood forecasting in a Canadian Prairie watershed, *Hydrol. Sci. J.*, 63(8), 1133–1149,
1026 doi:10.1080/02626667.2018.1474219, 2018.

1027 Wheeler, H. and Gober, P.: Water security in the Canadian Prairies: Science and management challenges,
1028 *Philos. Trans. R. Soc. A Math. Phys. Eng. Sci.*, 371(2002), doi:10.1098/rsta.2012.0409, 2013.

1029 Whitfield, P. H., Shook, K. R., and Pomeroy, J. W.: Spatial patterns of temporal changes in Canadian Prairie
1030 streamflow using an alternative trend assessment approach, *J. Hydrol.*, 582(December 2019),
1031 doi:10.1016/j.jhydrol.2020.124541, 2020.

1032 Withey, P. and van Kooten, G. C.: The effect of climate change on optimal wetlands and waterfowl
1033 management in Western Canada, *Ecol. Econ.*, 70(4), 798–805, doi:10.1016/j.ecolecon.2010.11.019,
1034 2011.

1035 Wolfe, J. D., Shook, K. R., Spence, C., and Whitfield, C. J.: A watershed classification approach that looks
1036 beyond hydrology: Application to a semi-arid, agricultural region in Canada, *Hydrol. Earth Syst.*
1037 *Sci.*, 23(9), 3945–3967, doi:10.5194/hess-23-3945-2019, 2019.

1038 Van Hoy, D. F., Mahmood, T. H., Todhunter, P. E., and Jeannotte, T. L.: Mechanisms of Cold Region
1039 Hydrologic Change to Recent Wetting in a Northern Glaciated Landscape, *Water Resour. Res.*, 56,
1040 1–28, <https://doi.org/10.1029/2019WR026932>, 2020.

1041 Valeo, C., Xiang, Z., Bouchart, F. J.-C., Yeung, P., and Ryan, M. C.: Climate Change Impacts in the Elbow
1042 River Watershed, *Canadian Water Resources Journal*, 32:4, 285-302, DOI: 10.4296/cwrj3204285,
1043 2007.

1044 Zhang, H., Huang, G. H., Wang, D., and Zhang, X.: Uncertainty assessment of climate change impacts on
1045 the hydrology of small prairie wetlands, *J. Hydrol.*, 396(1–2), 94–103,
1046 doi:10.1016/j.jhydrol.2010.10.037, 2011.

1047 Zhang, Z., Bortolotti, L. E., Li, Z., Armstrong, L. M., Bell, T. W., and Li, Y.: Heterogeneous Changes to
1048 Wetlands in the Canadian Prairies Under Future Climate, *Water Resour. Res.*, 57(7), 1–16,
1049 doi:10.1029/2020WR028727, 2021.